Electrostatic interactions between anisotropic particles

Harshit Joshi *
International Centre for Theoretical Sciences, Bengaluru (ICTS-TIFR), Karnataka 560089, India

Anubhab Roy
Department of Applied Mechanics, Indian Institute of Technology Madras, Chennai, Tamil Nadu 600036, India

(Received 10 January 2025; accepted 25 February 2025; published 20 March 2025)

We investigate the electrostatic interactions between two charged anisotropic conductors using a combination of asymptotic and numerical methods. For widely separated particles, we employ the method of reflections to analyze the interactions. Although the formulation applies to conductors of arbitrary shapes, it is specifically implemented for spheroid-sphere systems to capture anisotropy effects in a simple configuration. In near-contact cases with axisymmetric configurations, the lubrication approximation is used to extend the analysis. Additionally, we develop a boundary integral method to study particle interactions at arbitrary separations, validating the results with asymptotic solutions for both near and far fields. We derive analytical expressions for the electrostatic force and torque on a spheroid due to another spheroid in the far-field regime. When combined with hydrodynamic effects, the electrostatic torque competes with the hydrodynamically favorable alignments of a pair of settling spheroids in certain regions while reinforcing them in others. Consequently, the inclusion of electrostatic effects may influence the instability observed in dilute suspensions of spheroids.

DOI: 10.1103/PhysRevE.111.035410

I. INTRODUCTION

Electrostatic interactions play a significant role in various natural and industrial processes, influencing behaviors across systems as diverse as atmospheric phenomena, biological assemblies, and colloidal suspensions [1–5]. In atmospheric science, for example, electrostatic forces are integral to cloud formation, where charged particles, including ice crystals and droplets, cluster and interact in complex ways that impact precipitation and cloud evolution [5]. Even droplets bearing the same charge can coalesce due to electrostatic induction effects, enabling attraction through localized polarization despite net repulsion between like charges [6–8]. This phenomenon, while extensively studied for simple geometries like spherical particles [9,10], is less understood in realistic cases involving anisotropic interactions and irregular shapes.

One of the simplest nonspherical shapes relevant in such studies is the spheroid, a shape commonly found in atmospheric ice crystals and approximations of biological and industrial particles. To better understand the interaction of such anisotropic objects, this study focuses on the electrostatic interaction between a conducting sphere and a spheroidal body. Specifically, this work presents a calculation of the electrostatic torque exerted on a spheroid by a nearby sphere, which represents a key contribution to modeling how such particles align and rotate under electrostatic forces. This torque, together with the corresponding interaction forces, could be incorporated into cloud microphysics models to complement hydrodynamic models that already consider droplet interactions driven by hydrodynamic forces [11]. In mixed-phase clouds, ice crystals collide with supercooled liquid droplets, becoming coated in a process called riming [12,13]. Riming is a critical process in the formation of precipitation-sized hydrometeors within clouds. Precise calculation of the interaction forces between the anisotropic hydrometeor and the droplet is vital for accurately determining the collision efficiency during the riming process between ice particles and supercooled droplets.

Electrical charging mechanisms in clouds involve complex interactions between droplets, ice crystals, and graupel particles, driven by a combination of collisions and environmental factors [5,7]. Field measurements in weakly electrified clouds show that ice crystal and droplet charges are proportional to their surface areas [14–16]. Mechanisms such as inductive charging, which arises from the polarization of particles in an existing electric field, and convective charging, where vertical air currents separate charged particles, also play a role in cloud electrification. However, the most significant mechanism is collisional charging, where charge transfer occurs during collisions between particles. For example, when supercooled water droplets freeze upon colliding with graupel particles, charge separation occurs due to differences in ion mobility, thermal properties, and the rime accretion electrification process [5,17–19]. In these processes, smaller ice crystals (10–100 μm) typically acquire a positive charge, while larger graupel or hailstones (1–5 mm) gain a negative charge, with the charge separated during each collision ranging from 10^{-16} to 10^{-12} C, depending on factors such as temperature, impact velocity, and the presence of supercooled water. Since collisional charging is the dominant process

*Contact author: harshit.joshi@icts.res.in

driving charge separation in clouds, and ice crystals are inherently anisotropic, understanding the role of particle anisotropy and their electrostatic interactions is crucial for improving our understanding of cloud electrification.

Analytical methods for determining electrostatic forces and torques on multiple conductors are limited to simple geometries such as sphere-sphere [20] and spheroid-spheroid in specific configurations [21]. In this work we extend this computation to two spheroidal conductors in a generic configuration in the far-field regime. The far-field calculations are carried out using the method of reflections, widely used in the problems of microhydrodynamics [22], and described in detail in Appendix C. Having obtained the electrostatic interaction between two spheroids, we explore the role of anisotropy in the simpler, yet unexplored electrostatic interaction between a spheroid and a sphere. This system is sufficient to capture the anisotropy in the problem and provides a manageable parameter space over which relevant quantities can be analyzed. We use a boundary integral method (BIM) to uniformly capture the electrostatic interaction in both far- and near-field regimes. We compare the BIM with the method of reflections to determine the proximity at which the method of reflections starts to lose accuracy for closely spaced conductors. We derive an analytical expression for the electrostatic force and torque in the far-field regime using the first reflection, applicable to both spheroid-sphere and spheroid-spheroid systems. It is speculated that incorporating electrostatic torque in a dilute suspension of charged spheroids may modify the previously observed instability in density fluctuations of uncharged spheroids.

II. METHODS

A. Potential matrix formulation

The electrostatic interaction between multiple conductors involves determining the potential on the surface of each conductor, given the total charge on each conductor. This information is sufficient to determine the total electrostatic energy of the system and hence compute forces and torques on each conductor. The governing equation for the potential outside the conductors is simply the Laplace equation. The complexity of the problem comes from the boundary conditions that need to be satisfied at the surface of each conductor. The linearity of governing equations of electrostatics implies a linear relationship between the total charges on each conductor and the potential on their surfaces. The proportionality constant is called the potential matrix $\mathbf{\Phi}_M$ [23–27], which only depends on the permittivity of free space ε_0, size, and the geometry of the conductors [28]. Since we are interested in two-body electrostatic interaction, the connection between charges Q_1 and Q_2 and the potentials V_1 and V_2 on the surface of the conductors S_1 and S_2 is given by

$$\begin{pmatrix} V_1 \\ V_2 \end{pmatrix} = \frac{1}{4\pi\varepsilon_0 a}\begin{pmatrix} \Phi_{11} & \Phi_{12} \\ \Phi_{21} & \Phi_{22} \end{pmatrix}\begin{pmatrix} Q_1 \\ Q_2 \end{pmatrix}, \tag{1}$$

where a is the typical size of the conductors and Φ_{ij}, $i, j \in \{1, 2\}$, are the dimensionless elements of the potential matrix, $\mathbf{\Phi}_M$, which depends on the relative position, orientations, and the geometry of the two conductors. Using the reciprocal theorem, one can show that the potential matrix is symmetric, i.e., $\mathbf{\Phi}_M^T = \mathbf{\Phi}_M$ [23–25].

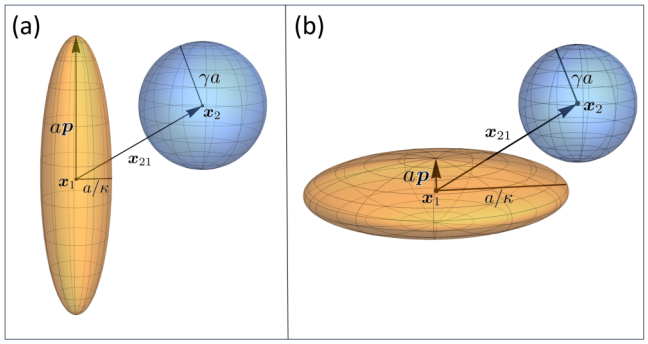

FIG. 1. A schematic illustrating the geometric setup for electrostatic pair interactions between a spheroid and a sphere in a generic, nonaxisymmetric configuration. The unit vector $\boldsymbol{p}$ represents the orientation of the spheroid, with a denoting the size of the spheroid, κ denoting its aspect ratio, and γ denoting the size ratio of the sphere to spheroid. (a) Prolate spheroid and a sphere. (b) Oblate spheroid and a sphere.

The subsequent sections are concerned with the calculation of the potential matrix $\mathbf{\Phi}_M$ of a spheroid-sphere system in the far-field, near-field, and uniformly valid regimes. Before undertaking full numerical calculations, we will first examine two distinct asymptotic limits: when the particles are widely separated and when they are nearly touching.

B. Far-field interactions: Method of reflections

The method of reflection is an iterative approach that progressively satisfies boundary conditions on surfaces by incorporating corrections from each preceding iteration [22]. The solution to each iteration is given by the multipole expansions, which yields a perturbation series in a/R, where a is the typical size of the conductors and R is their typical separation. A detailed description of this method in the context of electrostatics is given in Appendix C. Here, we briefly mention the common terminologies of this method. Consider a *prolate* spheroid S_1, carrying a total charge Q_1, centered at $\boldsymbol{x}_1$ with a as the distance from its center to the pole along the symmetry axis denoted by the unit vector $\boldsymbol{p}$ (see Fig. 1). The spheroid's aspect ratio $\kappa(>1)$ is defined as the ratio of a to its equatorial radius lying perpendicular to $\boldsymbol{p}$, and its eccentricity is $e = \sqrt{1-\kappa^{-2}}$. The surface of this prolate spheroid is given by

$$(\boldsymbol{x}-\boldsymbol{x}_1)\cdot\left[\frac{\boldsymbol{pp}}{a^2} + \frac{(\mathbb{1}-\boldsymbol{pp})}{a^2\kappa^{-2}}\right]\cdot(\boldsymbol{x}-\boldsymbol{x}_1) = 1, \quad \boldsymbol{x}\in S_1. \tag{2}$$

Here $\mathbb{1}$ is the identity tensor. The second conductor is a sphere S_2 centered at $\boldsymbol{x}_2$ with radius γa and total charge Q_2, the surface of which is given by

$$(\boldsymbol{x}-\boldsymbol{x}_2)\cdot(\boldsymbol{x}-\boldsymbol{x}_2) = (\gamma a)^2, \quad \boldsymbol{x}\in S_2. \tag{3}$$

The relative separation vector between them is $\boldsymbol{x}_{21} \equiv \boldsymbol{x}_2 - \boldsymbol{x}_1 \equiv -\boldsymbol{x}_{12}$. The *first reflection* approximation accounts for the correction of potential fields produced by the sphere and spheroids as if they were isolated. The corresponding potential matrix in this case is accurate only up to $O(a/R)$. The

elements of the potential matrix for a *prolate spheroid* are given by

$$\Phi_{11}^{(1)} = e^{-1}\text{arctanh}e, \tag{4a}$$

$$\Phi_{12}^{(1)} = \Phi_{21}^{(1)}(\boldsymbol{x}_{12}, \boldsymbol{p}) = \frac{1}{2e}\ln\left(\frac{z_{12} - ae - R_-}{z_{12} + ae - R_+}\right), \tag{4b}$$

$$\Phi_{22}^{(1)} = \gamma^{-1}, \tag{4c}$$

where

$$R_\pm \equiv \sqrt{\rho_{12}^2 + (z_{12} \pm ae)^2}, \tag{5a}$$

$$\rho_{12}^2 \equiv \boldsymbol{x}_{12}\cdot(\mathbb{1} - \boldsymbol{pp})\cdot\boldsymbol{x}_{12}, \tag{5b}$$

$$z_{12} \equiv \boldsymbol{x}_{12}\cdot\boldsymbol{p}. \tag{5c}$$

Here we use the notation $\Phi_{ij}^{(n)}$ to represent the ijth element of the potential matrix up to the nth reflection. Note that up to the first reflection correction the effect of interaction is only captured by the off-diagonal terms. Now, the *second reflection* accounts for the correction in the potential fields produced in response to the first reflected fields. The corresponding potential matrix in this case is accurate up to $O(a^4/R^4)$, with the elements for a prolate spheroid given by

$$\Phi_{11}^{(2)}(\boldsymbol{x}_{12}, \boldsymbol{p}) = \Phi_{11}^{(1)} - \frac{a^2\gamma^3}{4e^2}\left[\left(\frac{1}{R_-} - \frac{1}{R_+}\right)^2 + \rho_{12}^2\left(\frac{1}{R_+(z_{12} + ae - R_+)} - \frac{1}{R_-(z_{12} - ae - R_-)}\right)^2\right], \tag{6a}$$

$$\Phi_{12}^{(2)}(\boldsymbol{x}_{12}, \boldsymbol{p}) = \Phi_{21}^{(2)}(\boldsymbol{x}_{12}, \boldsymbol{p}) = \Phi_{12}^{(1)}(\boldsymbol{x}_{12}, \boldsymbol{p}), \tag{6b}$$

$$\begin{aligned}\Phi_{22}^{(2)}(\boldsymbol{x}_{12}, \boldsymbol{p}) = \Phi_{22}^{(1)} - \frac{9}{4a^2e^6}\Bigg[&X_p^C\left\{R_- - R_+ + z_{12}\ln\left(\frac{z_{12} - ae - R_-}{z_{12} + ae - R_+}\right)\right\}^2 \\ &+ \frac{1}{4}Y_p^C\left\{\frac{z_{12}}{\rho_{12}}(R_- - R_+) + \frac{ae}{\rho_{12}}(R_- + R_+) - \rho_{12}\ln\left(\frac{z_{12} - ae - R_-}{z_{12} + ae - R_+}\right)\right\}^2\Bigg],\end{aligned} \tag{6c}$$

where

$$X_p^C \equiv \frac{e^3}{3}(\text{arctanh}\, e - e)^{-1}, \tag{7a}$$

$$Y_p^C \equiv \frac{2e^3}{3}\left(\frac{e}{1 - e^2} - \text{arctanh}e\right)^{-1}. \tag{7b}$$

Now consider an *oblate* spheroid S_1 centered at $\boldsymbol{x}_1$ with a as the distance from its center to the pole along the symmetry axis denoted by the unit vector $\boldsymbol{p}$ (see Fig. 1). Its aspect ratio is $\kappa(<1)$, with an eccentricity of $e = \sqrt{1 - \kappa^2}$ and it carries a total charge Q_1. The surface of this oblate spheroid S_1 is again given by (2) with the only difference being $\kappa < 1$. The second conductor S_2 is again a sphere of radius γa, centered at $\boldsymbol{x}_2$, carrying a total charge Q_2. To obtain the corresponding potential matrix of the spheroid-sphere system we use the eccentricity transformation $e \to \frac{ie}{\sqrt{1-e^2}}$ on the corresponding expressions of the prolate spheroid [29]. Therefore, for an oblate spheroid and a sphere, we have

$$\Phi_{11}^{(1)} = \frac{\kappa\arcsin e}{e}, \tag{8a}$$

$$\Phi_{12}^{(1)} = \Phi_{21}^{(1)}(\boldsymbol{x}_{12}, \boldsymbol{p}) = \frac{\kappa}{e}\text{arccot}\left(\frac{z_{12} - u}{v - ae/\kappa}\right), \tag{8b}$$

$$\Phi_{22}^{(1)} = \gamma^{-1}, \tag{8c}$$

where z_{12} is given by Eq. (5) and u and v are given by

$$u \equiv \sqrt{\frac{\mu}{2} + \sqrt{\frac{\mu^2}{4} + \frac{a^2e^2}{\kappa^2}z_{12}^2}}; \quad \mu \equiv |\boldsymbol{x}_{12}|^2 - \frac{a^2e^2}{\kappa^2}, \tag{9a}$$

$$v \equiv \frac{aez_{12}}{\kappa u}. \tag{9b}$$

Similarly, the second reflection corrections are given by

$$\Phi_{11}^{(2)}(\boldsymbol{x}_{12},\boldsymbol{p}) = \Phi_{11}^{(1)} - \frac{\kappa^2 a^2\gamma^3}{4e^2}\left[\left(\frac{2v}{u^2+v^2}\right)^2 + \rho_{12}^2\left\{\frac{4ae\kappa^{-1}z_{12} - 2(z_{12}v + ae\kappa^{-1}u)}{(u^2+v^2)[(z_{12}-u)^2 + (ae\kappa^{-1}-v)^2]}\right\}^2\right], \tag{10a}$$

$$\Phi_{12}^{(2)}(\boldsymbol{x}_{12},\boldsymbol{p}) = \Phi_{21}^{(2)}(\boldsymbol{x}_{12},\boldsymbol{p}) = \Phi_{12}^{(1)}(\boldsymbol{x}_{12},\boldsymbol{p}), \tag{10b}$$

$$\Phi_{22}^{(2)}(\boldsymbol{x}_{12},\boldsymbol{p}) = \Phi_{22}^{(1)} - \frac{9\kappa^6}{a^2e^6}\left[X_o^C\left\{v - z_{12}\mathrm{arccot}\left(\frac{z_{12}-u}{v-ae\kappa^{-1}}\right)\right\}^2 + \frac{1}{4}Y_o^C\left\{\frac{ae\kappa^{-1}u - z_{12}v}{\rho_{12}} - \rho_{12}\mathrm{arccot}\left(\frac{z_{12}-u}{v-ae\kappa^{-1}}\right)\right\}^2\right], \tag{10c}$$

where

$$X_o^C \equiv \frac{e^3}{3}[e(1-e^2) - (1-e^2)^{3/2}\arcsin e]^{-1}, \tag{11a}$$

$$Y_o^C \equiv \frac{2e^3}{3}[e(1-e^2)^2 - (1-e^2)^{3/2}\arcsin e]^{-1}. \tag{11b}$$

The potential matrix for two spherical conductors can be obtained by taking the limit $e \to 0$ in the potential matrix expression for a prolate spheroid. Therefore, for a spherical conductor, S_1, of radius a, centered at $\boldsymbol{x}_1$, and another spherical conductor, S_2, of radius γa, centered at $\boldsymbol{x}_2$, the elements of the potential matrix up to the second reflection are given by

$$\Phi_{11}^{(2)}(|\boldsymbol{x}_{21}|) = 1 - \frac{\gamma^3 a^4}{|\boldsymbol{x}_{21}|^4}, \tag{12a}$$

$$\Phi_{12}^{(2)}(|\boldsymbol{x}_{21}|) = \Phi_{21}^{(2)}(|\boldsymbol{x}_{21}|) = \frac{1}{|\boldsymbol{x}_{21}|}, \tag{12b}$$

$$\Phi_{22}^{(1)}(|\boldsymbol{x}_{21}|) = \frac{1}{\gamma} - \frac{a^4}{|\boldsymbol{x}_{21}|^4}. \tag{12c}$$

C. Near contact interaction: Lubrication approximation

Using the lubrication approximation for the spheroid-sphere system in the axisymmetric configuration involves solving the Laplace equation for the potential field $\phi(\boldsymbol{x})$ near the gap of thickness $a\epsilon$ between the conductors. Using polar coordinates with z coordinate along the symmetry axis $\boldsymbol{p}$ and r coordinate transverse to $\boldsymbol{p}$, the boundary value problem to be solved is

$$\nabla^2\phi = \frac{\partial^2\phi}{\partial z^2} + \frac{1}{r}\frac{\partial}{\partial r}\left(r\frac{\partial\phi}{\partial r}\right) = 0, \tag{13a}$$

$$\phi = \begin{cases} V_1, & z = h_1(r) \\ V_2, & z = h_2(r). \end{cases} \tag{13b}$$

The surface of the spheroid and the sphere can be expanded as

$$\frac{h_1(r)}{a\epsilon} = 1 + \frac{\kappa^2 r^2}{2\epsilon a^2} + \frac{1}{8}\frac{\kappa^4 r^4}{\epsilon a^4} + O\left(\frac{\kappa^6 r^6}{\epsilon a^6}\right), \tag{14a}$$

$$\frac{h_2(r)}{a\epsilon} = -\frac{1}{2}\frac{r^2}{\epsilon\gamma a^2} - \frac{1}{8}\frac{r^4}{\epsilon\gamma^3 a^4} + O\left(\frac{r^6}{\epsilon\gamma^5 a^6}\right). \tag{14b}$$

Defining the stretched coordinates $R \equiv r/(a\sqrt{\epsilon})$ and $Z \equiv z/(a\epsilon)$, we have

$$H_1(R) = 1 + \frac{\kappa^2 R^2}{2} + \frac{\epsilon\kappa^4 R^4}{8} + O(\epsilon^2), \tag{15a}$$

$$H_2(R) = -\frac{R^2}{2\gamma} - \frac{\epsilon R^4}{8\gamma^3} + O(\epsilon^2). \tag{15b}$$

Rewriting the Laplace equation in terms of the stretched coordinates, we have

$$\frac{\partial^2\phi}{\partial Z^2} + \frac{\epsilon}{R}\frac{\partial}{\partial R}\left(R\frac{\partial\phi}{\partial R}\right) = 0, \tag{16a}$$

$$\phi = \begin{cases} V_1, & Z = H_1(R) \\ V_2, & Z = H_2(R). \end{cases} \tag{16b}$$

The solution can be expanded in the perturbation series as $\phi = \phi_0 + \epsilon\phi_1 + O(\epsilon^2)$. The total charge Q_1 and Q_2 on the spheroid S_1 and sphere S_2 are given by

$$Q_\alpha = -\varepsilon_0 \oint_{S_\alpha} \nabla\phi\cdot\hat{\boldsymbol{n}}_\alpha dS_\alpha, \quad \alpha \in \{1,2\}, \tag{17}$$

where $\hat{\boldsymbol{n}}_\alpha$ represents the unit normal pointing out of the surface S_α. The electrostatic force $\boldsymbol{F}_1$ on the spheroid is given by

$$\boldsymbol{F}_1 = \frac{\varepsilon_0}{2}\oint_{S_1} |\nabla\phi\cdot\hat{\boldsymbol{n}}_1|^2\hat{\boldsymbol{n}}_1 dS_1. \tag{18}$$

Using the zeroth-order solution ϕ_0, the charge difference $\Delta Q_{12} = Q_1 - Q_2$ is given by

$$\Delta Q_{12} = \frac{4\pi a\varepsilon_0\gamma\Delta V_{12}}{1+\gamma\kappa^2}\left[\ln\left(\frac{1+\gamma\kappa^2}{2\gamma\kappa\epsilon}\right) + \delta\right] + O(\epsilon), \tag{19}$$

where $\Delta V_{12} \equiv V_1 - V_2$ and δ is an $O(1)$ constant which has to be determined using the outer solution. The weak logarithmic singularity is insufficient to overpower the δ correction, even at very small separations ϵ, and therefore δ cannot be neglected. The forces $\boldsymbol{F}_1$ and $\boldsymbol{F}_2$ are given by

$$\boldsymbol{F}_1 = -\boldsymbol{F}_2 \sim \frac{-\hat{\boldsymbol{x}}_{12}(1+\gamma\kappa^2)\Delta Q_{12}^2}{16\pi a^2\varepsilon_0\gamma\epsilon\left[\ln\left(\frac{1+\gamma\kappa^2}{2\gamma\kappa\epsilon}\right) + \delta\right]^2}. \tag{20}$$

Note that for unequal total charges $\Delta Q_{12} \neq 0$, the electrostatic forces at close range are attractive, regardless of whether the conductors carry like or unlike charges. The force expression (20) reduces to the near contact force between two spheres for $\kappa = 1$ ([20,30]).

We rewrite Eq. (19) in terms of δ as

$$\delta = \lim_{\epsilon\to 0}\left\{\frac{(1+\gamma\kappa^2)\Delta Q_{12}}{4\pi a\varepsilon_0\gamma\,\Delta V_{12}} - \ln\left(\frac{1+\gamma\kappa^2}{2\gamma\kappa\epsilon}\right)\right\}. \tag{21}$$

We shall use the BIM to evaluate the right-hand side of the above equation for $\epsilon \ll 1$ and thus obtain δ. The numerical values of the right-hand side of Eq. (21) will have small variations with ϵ even when $\epsilon \ll 1$. This is due to the fact that the numerical errors in the BIM increases as the surfaces approach each other [31,32]. The error in the numerical measurement of δ, i.e., $\Delta\delta$, gives error on the forces $|\Delta F|$ [see Eq. (20)] as

$$|\Delta F| = |\boldsymbol{F}_1|\left|\frac{2\Delta\delta}{\left[\ln\left(\frac{1+\gamma\kappa^2}{2\gamma\kappa\epsilon}\right)+\delta\right]}\right|. \tag{22}$$

Note that the relative error in the forces decreases with ϵ. Once the δ is obtained, the lubrication force (20) gives electrostatic forces in the configurations where the minimum separation between the conductors becomes vanishingly small.

D. Boundary integral method

The method of reflections is primarily effective for far-field interactions. Achieving higher accuracy requires additional reflections, but each successive reflection adds significant complexity in the analytical expressions. To compute the interactions in both far- and near-field regimes numerically, we use the BIM. The BIM formulation is well established for various linear partial differential equations, including the Laplace equation [33–35]. A brief formulation of the BIM for the electrostatic problem with total charges specified on each conductor is given in Appendix D. Here we outline the main integral equations to be solved numerically to compute the potential matrix for a spheroid S_1 (both prolate and oblate) and a sphere S_2. The potentials on the surface of the conductors are given by

$$\varepsilon_0 V_\alpha = \frac{1}{|S_\alpha|}\oint_{S_\alpha} q_\alpha(\boldsymbol{x})dS_\alpha(\boldsymbol{x}); \quad \alpha\in\{1,2\}, \tag{23}$$

where $|S_\alpha|$ is the surface area of the conductor S_α. The fields q_α are obtained by solving the second-kind integral equation on every point $\boldsymbol{x}_{s\alpha}$ on the surface of conductor S_α:

$$\begin{bmatrix}\mathcal{L}^d_{11}+\mathcal{P}^c_{11}+\mathbb{I} & \mathcal{L}^d_{12}\\ \mathcal{L}^d_{21} & \mathcal{L}^d_{22}+\mathcal{P}^c_{22}+\mathbb{I}\end{bmatrix}\begin{bmatrix}q_1\\ q_2\end{bmatrix} = \begin{bmatrix}Q_1\mathcal{G}(\boldsymbol{x}_{s1},\boldsymbol{x}_1)+Q_2\mathcal{G}(\boldsymbol{x}_{s1},\boldsymbol{x}_2)\\ Q_1\mathcal{G}(\boldsymbol{x}_{s2},\boldsymbol{x}_1)+Q_2\mathcal{G}(\boldsymbol{x}_{s2},\boldsymbol{x}_2)\end{bmatrix}, \tag{24}$$

where Q_1 and Q_2 are the charges on the conductors S_1 and S_2, respectively, and $\mathcal{G}$ is the Green's function of the Laplacian, given by

$$\mathcal{G}(\boldsymbol{x},\boldsymbol{x}_0) \equiv \frac{1}{4\pi|\boldsymbol{x}-\boldsymbol{x}_0|}. \tag{25}$$

The integral operators are defined as

$$\mathcal{L}^d_{\alpha\beta}q_\beta(\boldsymbol{x}_s) \equiv 2\oint_{S_\beta} q_\beta(\boldsymbol{x})\hat{\boldsymbol{n}}_\beta\cdot\nabla_{\boldsymbol{x}}\mathcal{G}(\boldsymbol{x},\boldsymbol{x}_s)dS_\beta(\boldsymbol{x}), \tag{26a}$$

$$\mathcal{P}^c_{\alpha\beta}q_\beta \equiv \frac{1}{|S_\alpha|}\delta_{\alpha\beta}\oint_{S_\beta} q_\beta(\boldsymbol{x})dS_\beta(\boldsymbol{x}); \quad \boldsymbol{x}_s\in S_\alpha, \tag{26b}$$

TABLE I. The values of κ and γ used in the numerical calculations for the three systems—sphere-sphere, prolate spheroid-sphere, and oblate spheroid-sphere—are provided.

κ	1	4	0.25
γ	1	0.445	3.01

$\alpha,\beta\in\{1,2\}$. Equations (23) and (24) are used to determine the potential matrix. The integral equation (24) is solved using Generalized minimal residual method (GMRES) iterations [31,36] and the integrals on the surfaces are evaluated using the Gaussian quadrature [31,37].

E. Electrostatic force and torque

When particles carry an electric charge, they can experience strong mutual interactions. Precisely calculating the electric forces and torques acting on these charged particles is crucial across a wide range of physical systems, including biological cells, ice crystals, and granular materials. These force calculations are essential for predicting particle dynamics, such as their trajectories and the potential for aggregation. The electrostatic force and torque on each conductor can be computed by taking derivatives of the electrostatic energy of the system. The electrostatic energy of the spheroid-sphere system is given by

$$W(|\boldsymbol{x}_{21}|,\hat{\boldsymbol{x}}_{21}\cdot\boldsymbol{p}) = \tfrac{1}{2}\boldsymbol{Q}^T\cdot\boldsymbol{\Phi}_M(|\boldsymbol{x}_{21}|,\hat{\boldsymbol{x}}_{21}\cdot\boldsymbol{p})\cdot\boldsymbol{Q}, \tag{27}$$

with $\boldsymbol{Q}\equiv[Q_1 \quad Q_2]^T$, where the spheroid centered at $\boldsymbol{x}_1$ carries a total charge Q_1 and the sphere centered at $\boldsymbol{x}_2$ carries a total charge Q_2. Here $\hat{\boldsymbol{x}}_{21}$ is a unit vector along the separation vector $\boldsymbol{x}_{21}=\boldsymbol{x}_2-\boldsymbol{x}_1$. The differential change in the electrostatic energy upon differential change in the relative configuration is given by

$$dW = d\boldsymbol{x}_{21}\cdot\nabla_{21}W + d\boldsymbol{p}\cdot\nabla_p W. \tag{28}$$

The first term in Eq. (28) represents the negative of the work done by the electrostatic force on the sphere, $\boldsymbol{F}_2$, in moving the sphere by an amount $d\boldsymbol{x}_{21}$. Equivalently, it represents the negative of the work done by the electrostatic force on the spheroid, $\boldsymbol{F}_1$, in moving the spheroid by an amount $-d\boldsymbol{x}_{21}$. Therefore, the electrostatic forces on the conductors are given by

$$\boldsymbol{F}_1 = -\boldsymbol{F}_2 = \nabla_{\boldsymbol{x}_{21}}W(|\boldsymbol{x}_{21}|,\hat{\boldsymbol{x}}_{21}\cdot\boldsymbol{p}). \tag{29}$$

The second term shows that there is energy expense in changing the orientation of the spheroid. This shows that the electrostatic force on the spheroid does not act at its center. Thus, an electrostatic torque $\boldsymbol{T}_1$ acts on the spheroid about its center. The work done by the electrostatic force on the spheroid in changing its orientation can be written in terms of $\boldsymbol{T}_1$ as $\boldsymbol{T}_1\cdot\hat{\boldsymbol{n}}\,d\theta$, where $\hat{\boldsymbol{n}}$ is the axis about which $\boldsymbol{p}$ is rotated by an angle $d\theta$, i.e., $d\boldsymbol{p}=d\theta\,\hat{\boldsymbol{n}}\times\boldsymbol{p}$. Equating this to the second term in Eq. (28) gives the torque on the spheroid about its center as

$$\boldsymbol{T}_1 = -\boldsymbol{p}\times\nabla_{\boldsymbol{p}}W(|\boldsymbol{x}_{21}|,\hat{\boldsymbol{x}}_{21}\cdot\boldsymbol{p}). \tag{30}$$

The change in configuration due to the change in the orientation vector $\boldsymbol{p}=d\theta\,\hat{\boldsymbol{n}}\times\boldsymbol{p}$ is equivalent to keeping the

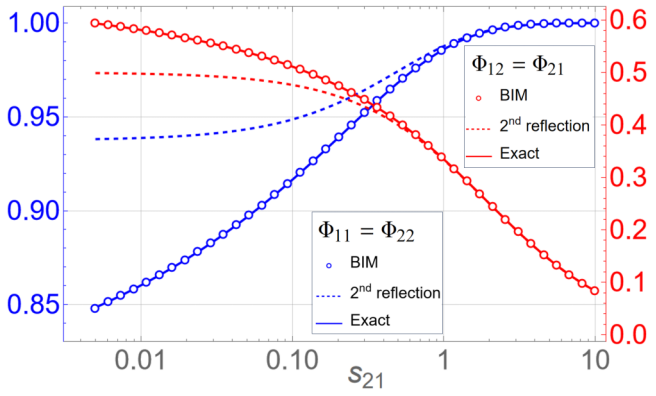

FIG. 2. Elements of the potential matrix Φ_M [see (1)] as a function of dimensionless minimum separation between the two spheres, $s_{21} = |\boldsymbol{x}_{21}|/a - 2$. The second reflection is decent up to the separations of the order of the size of the spheres. The exact result in terms of an infinite series can be found in [20].

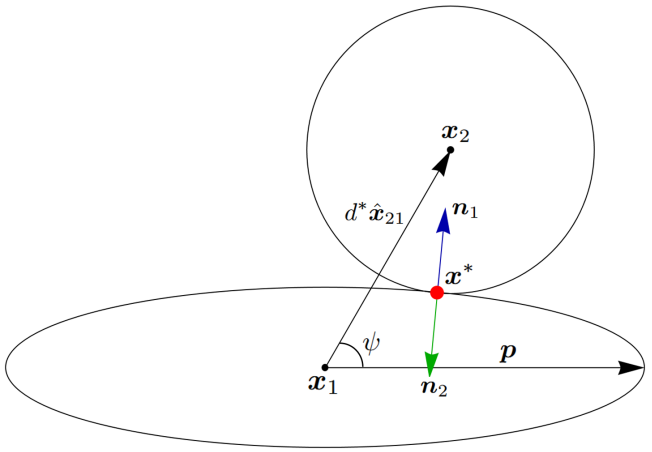

FIG. 3. A schematic showing the point of contact $\boldsymbol{x}^*$, the minimum distance $d^* = d_{\min}(\psi)$, and other relevant quantities for the case of a prolate spheroid and a sphere. The relative sizes of the conductors are proportional to their respective scales.

spheroid's orientation fixed but rotating the separation vector $\boldsymbol{x}_{21}$ about the spheroid's center, the opposite way, such that $d\boldsymbol{x}_{21} = -d\theta\,\hat{\boldsymbol{n}} \times \boldsymbol{x}_{21}$. The work done on the sphere by $\boldsymbol{F}_2$ in this case is simply, $\boldsymbol{F}_2 \cdot (-d\theta\,\hat{\boldsymbol{n}} \times \boldsymbol{x}_{21}) = -(\boldsymbol{x}_{21} \times \boldsymbol{F}_2) \cdot \hat{\boldsymbol{n}}\,d\theta \equiv \boldsymbol{T}_2 \cdot (-\hat{\boldsymbol{n}}\,d\theta)$. This shows the torque $\boldsymbol{T}_2$ on the sphere is simply

$$\boldsymbol{T}_2 = \boldsymbol{x}_{21} \times \boldsymbol{F}_2. \tag{31}$$

It is easy to see using Eqs. (29), (30), and (31) that $\boldsymbol{T}_1 = -\boldsymbol{T}_2$, and hence the total angular momentum of the system is conserved.

III. RESULTS

The parameter space to be explored contains the aspect ratio of spheroid κ and the ratio of the sphere's radius to the spheroid's semimajor axis γ for various configurations given by $\boldsymbol{x}_{21}$ and $\boldsymbol{p}$. For a given κ, we fix the value of γ such that the surface area of the spheroid is the same as that of the sphere. We look at three different aspect ratios $\kappa \in \{1, 4, 0.25\}$ (see Table I). The first case corresponds to the electrostatic interaction between two identical spheres, the results of which are well known [20]. This serves as a benchmark for our general results for spheroid-sphere interactions. The other two cases correspond to a prolate and an oblate spheroid, respectively.

A. Elements of the potential matrix

The elements of the potential matrix are defined in Eq. (1). For the case of two spheres ($\kappa = 1$), the exact expression is known from Lekner [20] and the second reflection results are given by Eq. (12). The comparison between second reflection, BIM, and exact expression shows that the second reflection performs well down to minimum separations between spheres comparable to their size (see Fig. 2). This also validates both the second reflection and the BIM.

For the case of electrostatic interactions between a spheroid and a sphere, the exact expressions of the potential matrix are not known, to the best of our knowledge. The potential matrix depends on both the separation between the conductors $|\boldsymbol{x}_{21}|$ and the relative configuration of the conductors $\cos(\psi) \equiv \hat{\boldsymbol{x}}_{21} \cdot \boldsymbol{p}$. The minimum separation between the centers of the conductors when they are just touching depends on ψ and is denoted by $d_{\min}(\psi)$. This minimum separation can be determined numerically by finding the roots $\boldsymbol{x}^*$ (point of contact) and d^* of the following equations:

$$\left|\frac{\boldsymbol{n}_1}{|\boldsymbol{n}_1|} + \frac{\boldsymbol{n}_2}{|\boldsymbol{n}_2|}\right| = 0, \tag{32a}$$

$$\left|\boldsymbol{x}^* + \gamma a \frac{\boldsymbol{n}_1}{|\boldsymbol{n}_1|} - d^*\hat{\boldsymbol{x}}_{21}\right| = 0, \tag{32b}$$

$$|\boldsymbol{n}_2|^2 = \gamma^2 a^2, \tag{32c}$$

$$\boldsymbol{x}^* \cdot (\boldsymbol{p} \times \hat{\boldsymbol{x}}_{21}) = 0, \tag{32d}$$

where $\boldsymbol{n}_1$ and $\boldsymbol{n}_2$ are the (non-normalized) normal vectors to the spheroid and sphere at $\boldsymbol{x}^*$, given by

$$\boldsymbol{n}_1 \equiv \left[\frac{\boldsymbol{p}\boldsymbol{p}}{a^2} + \frac{(\mathbb{1} - \boldsymbol{p}\boldsymbol{p})}{a^2\kappa^{-2}}\right] \cdot (\boldsymbol{x}^* - \boldsymbol{x}_1), \tag{33a}$$

$$\boldsymbol{n}_2 \equiv \boldsymbol{x}^* - \boldsymbol{x}_1 - d^*\hat{\boldsymbol{x}}_{21}. \tag{33b}$$

The four equations (32) uniquely determine $\boldsymbol{x}^*$ and $d^* = d_{\min}(\psi)$. Note that $\hat{\boldsymbol{x}}_{21}$ is given by a unit vector making an angle ψ with $\boldsymbol{p}$, which does not require specifying d^*.

A schematic representing $\boldsymbol{x}^*$, d^* and other relevant quantities is shown in Fig. 3.

The physical interpretations of Eqs. (32) are as follows:

(1) Equation (32a) enforces that the normals of the sphere and the spheroid are oriented antiparallel to each other.

(2) Equation (32b) ensures that $\boldsymbol{x}^*$ is the point of contact.

(3) Equation (32c) ensures that $\boldsymbol{x}^*$ lies at the surface of the sphere.

(4) Equation (32d) ensures that $\boldsymbol{x}^*$ lies in the plane defined by $\boldsymbol{p}$ and $\hat{\boldsymbol{x}}_{21}$.

For the case of a prolate spheroid and a sphere ($\kappa = 4$), the second reflection results are given in Eqs. (6). Figure 4 shows the elements of the potential matrix for a fixed $\psi = \pi/4$ as a function of dimensionless separation

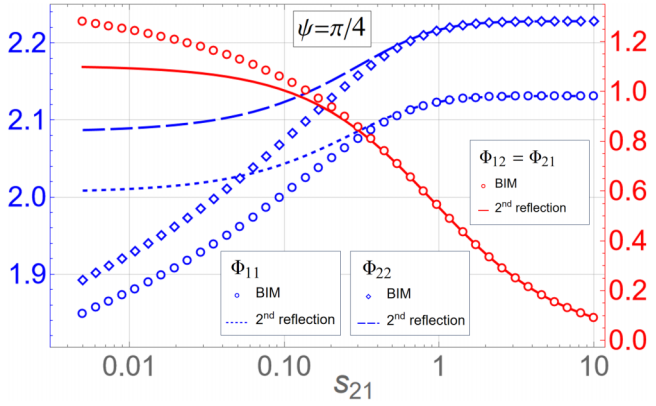

FIG. 4. Elements of the potential matrix Φ_M [see (1)] as a function of dimensionless separation between a prolate spheroid and a sphere, $s_{21} = [|\boldsymbol{x}_{21}| - d_{\min}(\psi)]/a$. Here $\psi \equiv \arccos(\hat{\boldsymbol{x}}_{21} \cdot \boldsymbol{p})$ and $d_{\min}$ is the dimensionless center-to-center distance between the prolate spheroid and the sphere when they are just in contact.

$s_{21} = [|\boldsymbol{x}_{21}| - d_{\min}(\psi)]/a$. The second reflection is reliable up to $s_{21} \sim 1$ (Fig. 5).

Similarly, for the case of an oblate spheroid and a sphere ($\kappa = 0.25$), the second reflection results [Eqs. (10)] are reliable up to $s_{21} \sim 4$ (see Fig. 5). This early deviation of the second reflection method from the BIM arises because the length scale used for s_{21} does not correspond to the larger dimension of the oblate spheroid, specifically the equatorial radius of the oblate spheroid $a\kappa^{-1}$.

B. Electrostatic force

Equation (29) is used to obtain the electrostatic force between the pair of conductors. This relies on differentiating the electrostatic energy obtained using the potential matrix. The exact results are available for the sphere-sphere case by [20]. The second reflection is again reliable up to $s_{21} \sim 1$. For very small separation $s_{21} \ll 1$, the BIM needs a large number of collocation points on the surfaces of the conductors to converge to the solution accurately. Lubrication approximation

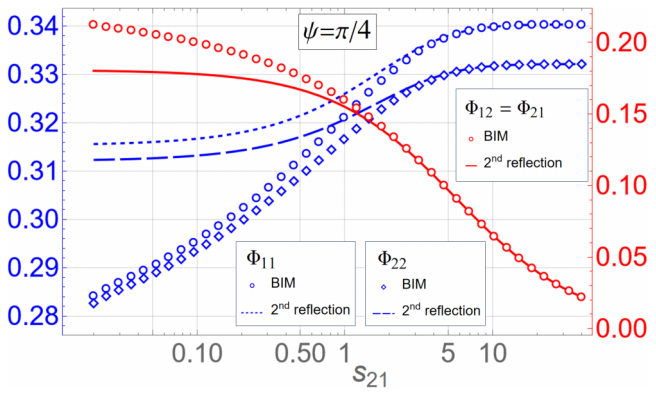

FIG. 5. Elements of the potential matrix Φ_M [see (1)] as a function of dimensionless separation between an oblate spheroid and a sphere, $s_{21} = [|\boldsymbol{x}_{21}| - d_{\min}(\psi)]/a$. Here $\psi \equiv \arccos(\hat{\boldsymbol{x}}_{21} \cdot \boldsymbol{p})$ and $d_{\min}$ is the dimensionless center-to-center distance between the oblate spheroid and the sphere when they are just in contact.

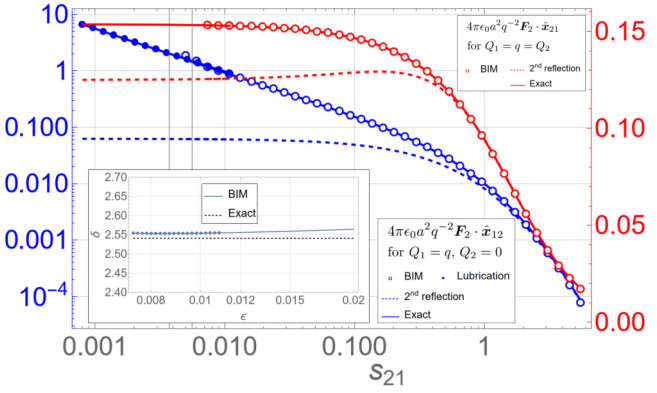

FIG. 6. Dimensionless force on the second sphere as a function of dimensionless minimum separation between the two spheres, $s_{21} = |\boldsymbol{x}_{21}|/a - 2$. Note that the force is attractive in the case of unequal charges ($\boldsymbol{F}_2 \cdot \boldsymbol{x}_{12} > 0$). The filled dots are obtained using the lubrication approximation [see Eq. (20)] with δ obtained using the BIM through Eq. (21). The inset shows δ as a function of ϵ, with the dots indicating the range of values over which δ is averaged to approximate it as a constant.

[Eq. (20)] has been used for $s_{21} \ll 1$, shown by the filled dots in Fig. 6, with the δ fitted using the BIM results.

The force acting on the sphere in the axisymmetric configuration ($\boldsymbol{p} \cdot \hat{\boldsymbol{x}}_{21}$) involving a prolate spheroid and a spherical conductor is shown in Fig. 7. The lubrication force is given by Eq. (20) with the δ fitted using the BIM results. Figure 8 shows the corresponding force for the case of an oblate spheroid and a sphere. Note that the electrostatic forces are attractive in the near contact case for unequal charges and grows unboundedly.

Figure 9 shows the variation of electrostatic force as a function of dimensionless separation s_{21} and the relative configuration ψ. This captures the effect of anisotropy of the problem.

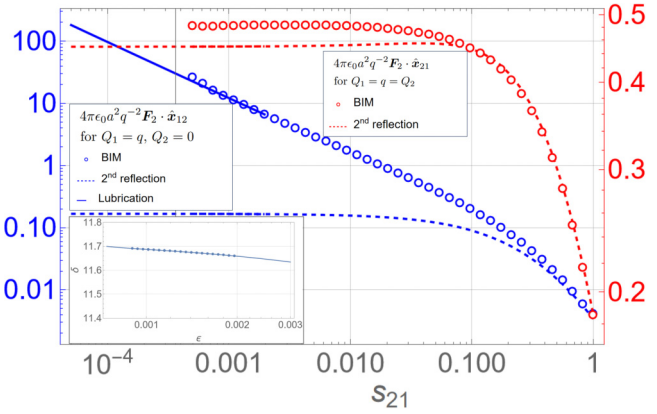

FIG. 7. Dimensionless force on the second sphere as a function of dimensionless separation between the prolate spheroid and the sphere, $s_{21} = |\boldsymbol{x}_{21}|/a - (1 + \gamma)$, in the axisymmetric configuration ($\boldsymbol{p} = \hat{\boldsymbol{x}}_{21}$). Note that the force is attractive in the case of unequal charges ($\boldsymbol{F}_2 \cdot \boldsymbol{x}_{12} > 0$). The lubrication approximation is obtained using Eq. (20) with δ obtained using the BIM through Eq. (21). The inset shows δ as a function of ϵ, with the dots indicating the range of values over which δ is averaged to approximate it as a constant.

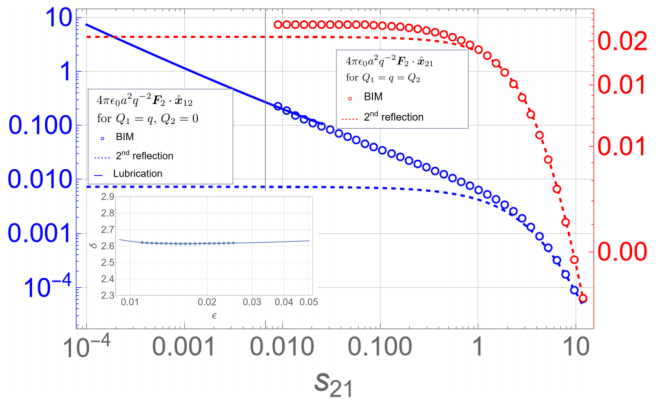

FIG. 8. Dimensionless force on the second sphere as a function of dimensionless separation between the oblate spheroid and the sphere, $s_{21} = |\boldsymbol{x}_{21}|/a - (1+\gamma)$, in the axisymmetric configuration ($\boldsymbol{p} = \hat{\boldsymbol{x}}_{21}$). Note that the force is attractive in the case of unequal charges ($\boldsymbol{F}_2 \cdot \boldsymbol{x}_{12} > 0$). The lubrication approximation is obtained using Eq. (20) with δ obtained using the BIM through Eq. (21). The inset shows δ as a function of ϵ, with the dots indicating the range of values over which δ is averaged to approximate it as a constant.

One is often interested in the dilute regime where particle separations are much larger than their size. In this regime, the first reflection is sufficient to capture the electrostatic force. Using Eqs. (29) and (4), the electrostatic force for the prolate spheroid and sphere system is given by

$$\boldsymbol{F}_2 \sim \frac{Q_1 Q_2}{8\pi\varepsilon_0 |\boldsymbol{x}_{21}|}\left\{\left(\frac{1}{R_+}+\frac{1}{R_-}\right)\hat{\boldsymbol{x}}_{21} + \frac{|\boldsymbol{x}_{21}|}{ae} \times \left(\frac{1-ae/R_+}{R_+ - ae - z_{12}} - \frac{1+ae/R_-}{R_- + ae - z_{12}}\right) \times (\mathbb{1} - \hat{\boldsymbol{x}}_{21}\hat{\boldsymbol{x}}_{21})\cdot \boldsymbol{p}\right\}, \tag{34}$$

where R_-, R_+, and z_{12} are given by Eq. (5). The corresponding electrostatic force due to the first reflection for the oblate spheroid and sphere system is given by

$$\boldsymbol{F}_2 \sim \frac{Q_1 Q_2}{4\pi\varepsilon_0 |\boldsymbol{x}_{12}|}\left\{\frac{a^2e^2 z_{12}^2 + \kappa^2 |\boldsymbol{x}_{12}|^2 u^2}{u(2u^2-\mu)(a^2e^2+\kappa^2u^2)}\hat{\boldsymbol{x}}_{12} - \frac{a^2e^2|\boldsymbol{x}_{12}|z_{12}}{u(2u^2-\mu)(a^2e^2+\kappa^2u^2)}(\mathbb{1} - \hat{\boldsymbol{x}}_{21}\hat{\boldsymbol{x}}_{21})\cdot \boldsymbol{p}\right\}, \tag{35}$$

where u and μ are given by Eq. (9). Note that the second term in the right-hand side of Eqs. (34) and (35) are the noncentral parts which arise due to the anisotropy of the systems and contribute to the electrostatic torques. Because these force expressions are valid only for large separations, they fail to account for the attractive forces between like charges that arise at short distances due to electrostatic induction.

Similarly, one can obtain a closed-form expression of force using Eq. (29) and the second reflection corrections to the potential matrix [Eqs. (6) and (10)] which is reliable up to $s_{21} = [|\boldsymbol{x}_{21}| - d_{\min}(\psi)]/a \sim 1$. The force from the second reflection can explain the attractive interaction between like charges; however, its accuracy diminishes at the separations where the attractive region begins.

C. Electrostatic torque

The electrostatic torque is the result of electrostatic forces on the conductors not being central. In other words, there is electrostatic energy cost in changing the orientation of the spheroid or changing the relative configuration ψ. Figure 10 shows the torque on the spheroid as a function of dimensionless separation s_{21} and ψ. As the separation decreases, the torque in the unequal charge case changes direction, indicating the onset of an attractive interaction between the conductors.

A quantity of interest in the dilute regime is the electrostatic torque between a pair of particles. The torque computed using the first reflection is accurate enough to capture the anisotropic effects in the far field. Using Eq. (34), one can obtain the torque for the prolate spheroid and sphere system,

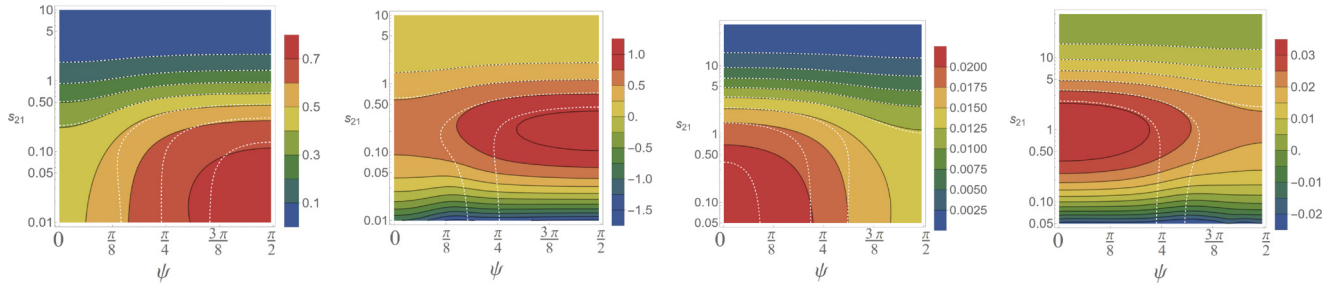

FIG. 9. Contour plot of dimensionless force along the separation vector, $4\pi\varepsilon_0 a^2 q^{-2}\boldsymbol{F}_2 \cdot \hat{\boldsymbol{x}}_{21}$, as a function of $\psi \equiv \arccos(\hat{\boldsymbol{x}}_{21}\cdot\boldsymbol{p})$ and $s_{21} = [|\boldsymbol{x}_{21}| - d_{\min}(\psi)]/a$. The white dotted lines are due to the second reflections. (a) The prolate spheroid has charge $Q_1 = q$ and the sphere has charge $Q_2 = q$, (b) The prolate spheroid has charge $Q_1 = q$ and the sphere has charge $Q_2 = 2q$, (c) The oblate spheroid has charge $Q_1 = q$ and the sphere has charge $Q_2 = q$, (d) The oblate spheroid has charge $Q_1 = q$ and the sphere has charge $Q_2 = 2q$.

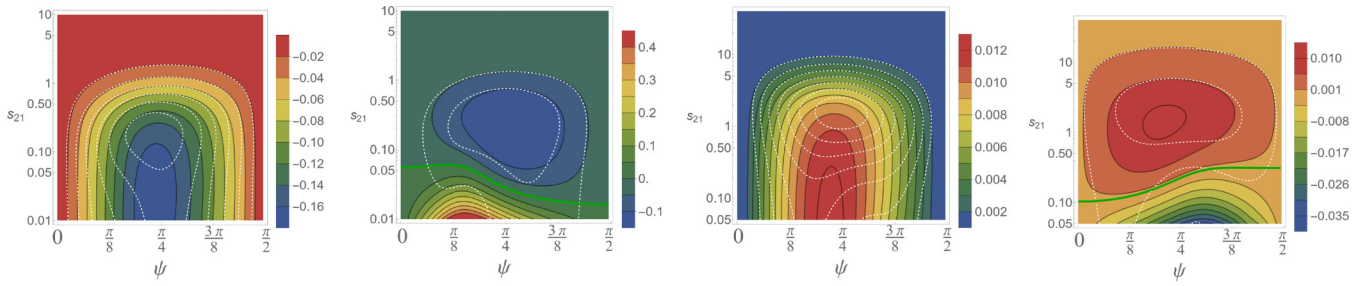

FIG. 10. Contour plot of dimensionless torque on spheroids about their center, $4\pi\varepsilon_0 a q^{-2}\boldsymbol{T}_1\cdot\hat{\boldsymbol{k}}$, as a function of $\psi \equiv \arccos(\hat{\boldsymbol{x}}_{21}\cdot\boldsymbol{p})$ and $s_{21} = [|\boldsymbol{x}_{21}| - d_{\min}(\psi)]/a$, where $\hat{\boldsymbol{k}}$ is a unit vector along $(\boldsymbol{p}\times\hat{\boldsymbol{x}}_{21})$. The white dotted lines are the due to the second reflections. The green curves in (b) and (d) separate the repulsive and the attractive regions. (a) The prolate spheroid has charge $Q_1 = q$ and the sphere has charge $Q_2 = q$, (b) The prolate spheroid has charge $Q_1 = q$ and the sphere has charge $Q_2 = 1.5q$, (c) The oblate spheroid has charge $Q_1 = q$ and the sphere has charge $Q_2 = q$, and (d) The oblate spheroid has charge $Q_1 = q$ and the sphere has charge $Q_2 = 1.5q$.

given by

$$\boldsymbol{T}_1 \sim \frac{Q_1 Q_2}{8\pi\varepsilon_0 ae}\left(\frac{1-ae/R_+}{R_+ - ae - z_{12}} - \frac{1+ae/R_-}{R_- + ae - z_{12}}\right)\boldsymbol{p}\times\boldsymbol{x}_{21}. \tag{36}$$

Similarly, using Eq. (35), one can obtain the torque for the oblate spheroid and sphere system, given by

$$\boldsymbol{T}_1 \sim \frac{Q_1 Q_2}{4\pi\varepsilon_0 u(2u^2-\mu)}\left(\frac{-a^2e^2z_{12}}{(a^2e^2+\kappa^2u^2)}\right)\boldsymbol{p}\times\boldsymbol{x}_{21}. \tag{37}$$

Here R_-, R_+, z_{12}, u, and μ are given by Eqs. (5) and (9). Note that the electrostatic forces and torques up to first reflection do not depend on the radius of the sphere [38]. This is because the electric field of a sphere, to a leading order in the far-field regime, is identical to that of a point charge placed at the center of the sphere. Now, if one has a pair of spheroids in the far-field regime, the electrostatic field of a spheroid can be approximated by the field due to a point charge located at its center. Therefore, in the far-field regime, the force and torque expressions [Eqs. (34)–(37)] serve as good approximations even for a spheroid-spheroid system. The comparison between torque due to first and second reflections and the BIM is shown in Fig. 11.

Studies have shown that electrostatic interactions, when combined with hydrodynamic interactions, can result in stable configurations for a pair of spheres [39]. An array of spheres and spheroids, as well as a dilute suspension of hydrodynamically interacting spheroids, have been found to be unstable to density perturbations [40–42]. The potential role of electrostatics in altering the stability of such systems remains unexplored.

In the like-charged anisotropic system, the electrostatic torque tends to align the spheroid in a broadside orientation relative to the separation vector $\boldsymbol{x}_{21}$, as illustrated in Fig. 12. In contrast, for oppositely charged particles, the stable orientation changes to thin side, as evident from Eqs. (36) and (37). These stable configurations contrast with the same system interacting hydrodynamically in a viscous flow [42], where

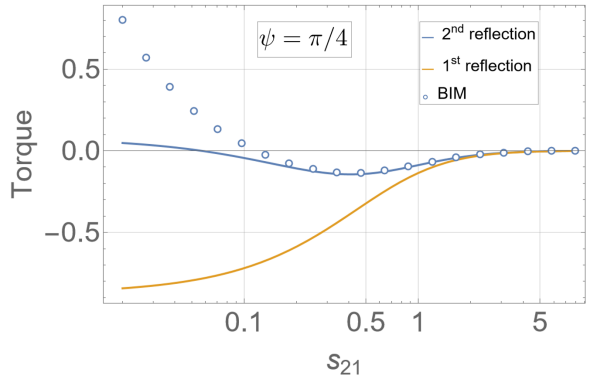

FIG. 11. Dimensionless torque on the prolate spheroid $4\pi\varepsilon_0 a q^{-2}\boldsymbol{T}_1\cdot\hat{\boldsymbol{k}}$ for $Q_1 = q$, $Q_2 = 2q$, as a function of separation $s_{21} = [|\boldsymbol{x}_{21}| - d_{\min}(\psi)]/a$ for a fixed $\psi \equiv \arccos(\hat{\boldsymbol{x}}_{21}\cdot\boldsymbol{p}) = \pi/4$, where $\hat{\boldsymbol{k}}$ is a unit vector along $(\boldsymbol{p}\times\hat{\boldsymbol{x}}_{21})$. The method of reflections aligns well with the BIM in the far field. The sign change in the torque at close range indicates an attractive electrostatic force due to induction. While the first reflection fails to predict this sign change, the second reflection captures it but loses accuracy in this close range.

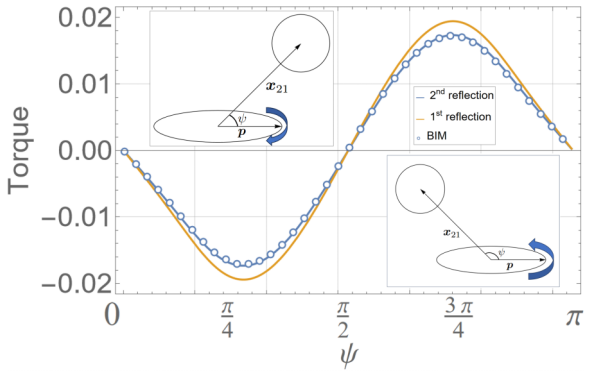

FIG. 12. Dimensionless torque on the prolate spheroid $4\pi\varepsilon_0 a q^{-2}\boldsymbol{T}_1\cdot\hat{\boldsymbol{k}}$ for $Q_1 = Q_2 = q$, as a function of $\psi \equiv \arccos(\hat{\boldsymbol{x}}_{21}\cdot\boldsymbol{p})$ for fixed $s_{21} = [|\boldsymbol{x}_{21}| - d_{\min}(\psi)]/a = 2$, where $\hat{\boldsymbol{k}}$ is a unit vector along $(\boldsymbol{p}\times\hat{\boldsymbol{x}}_{21})$. The change in the sign of the torque shows a stable configuration of the prolate spheroid and sphere system about $\psi = \pi/2$, as indicated in the insets.

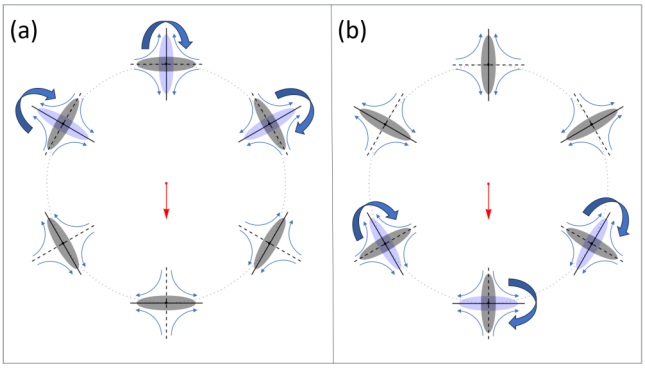

FIG. 13. Schematic showing the favorable orientations of a sedimenting spheroid interacting with another sedimenting spheroid through electrostatic and hydrodynamic interactions in the far-field regime. In the case of purely hydrodynamic interactions, one spheroid disturbs the flow as a force monopole (indicated by the red arrow) and causes the other spheroid to align along the extensional axis of the locally disturbed strain field (indicated by blue arrows). When electrostatic interactions are included, the electrostatic torque can either compete with or reinforce the hydrodynamic alignment, depending on whether the spheroid is in a trailing or a leading position. The black-shaded spheroids represent the favorable orientations due to electrostatic effects, while the light blue-shaded spheroids indicate those due to hydrodynamic effects. (a) For like-charged spheroids, the electrostatic torque competes with the hydrodynamic alignment for a trailing spheroid, as indicated by the arrows, while it reinforces the alignment for a leading spheroid. (b) For oppositely charged spheroids, the effects are reversed: the electrostatic torque competes with the hydrodynamic alignment for a leading spheroid and reinforces it for a trailing spheroid. This has implications in changing the stability of the dilute suspension of charged spheroids.

a spheroid falling above another one tends to align its thin side along their separation vector (see Fig. 13). As a result, in a dilute suspension of sedimenting charged spheroids, the hydrodynamic torque on a spheroid counteracts the electrostatic torque in some regions while reinforcing it in others. Consequently, incorporating electrostatic effects in such systems could alter the instability typically observed in purely hydrodynamic interactions [42].

IV. CONCLUSION

We have used the method of reflections to compute the potential matrix for sphere-sphere and spheroid-sphere conductors. This allows us to determine the electrostatic forces and torques acting on these conductors in the far-field regime. The formulation is general enough to be applied to arbitrary shapes as long as their singularity solutions are known, as discussed in the Appendixes. We also compute the electrostatic force under the lubrication approximation for nearly touching conductors in the axisymmetric configuration. To determine this close-range force accurately an order one constant δ is needed, which has been determined using the BIM. We also test the validity of the method of reflections with the BIM when the conductors are closely separated. The results show that second reflection works well until the separation is of the order of the size of the conductors.

The anisotropy of the problem of electrostatic interaction between a spheroid and a sphere results in the electrostatic torque. This torque tends to align the spheroid-sphere system in a manner different from the alignment due to pure hydrodynamic interactions [42] (see Fig. 13). This naturally prompts the question: how does the instability in a dilute suspension of sedimenting spheroids change when electrostatic effects are taken into account? Our work offers a foundational approach for computing electrostatic forces and torques on anisotropic particle pairs, demonstrated with example cases for a spheroid-sphere system, using the potential matrix. In the dilute regime, the simpler first-reflection expressions [Eqs. (36) and (37)] can be used to account for electrostatic interactions between spheroids and study the evolution of density perturbations in a spheroid suspension.

This work draws extensively on concepts from microhydrodynamics but deliberately excludes its effects to avoid additional complexity. However, in natural settings, microhydrodynamics and electrostatic effects often act together. Understanding the role of electrostatic forces in clustering within clouds, for instance, sheds light on the formation and dynamics of ice crystals and droplets. While hydrodynamic-driven clustering and orientation dynamics through turbulence has been extensively explored [43,44,47], the role of electrostatic interactions remains underexamined. Such insights can further our understanding of processes such as rain initiation, hail formation, and the structural evolution of clouds under varying atmospheric charge distributions. Beyond atmospheric science, applications extend to areas like the control of particulate matter in industrial filtration [2], the alignment of particles in electric fields in colloidal chemistry [4], and the behavior of charged proteins in biophysics [3], where electrostatic torques influence assembly and organization.

ACKNOWLEDGMENT

H.J. acknowledges support from the Department of Atomic Energy, Government of India, under Project No. RTI4001.

DATA AVAILABILITY

The data that support the findings of this article are openly available [45].

APPENDIX A: SINGULARITY SOLUTIONS FOR SPHEROIDS IN ELECTROSTATICS

The singularity solutions for the boundary value problems of the Laplace equation involve representing the solution in terms of the Green's function $\mathcal{G}$ of the Laplace equation and its higher derivatives located outside the domain of interest. The Green's function of the free-space Laplace equation in three dimensions satisfies

$$\nabla^2 \mathcal{G}(\boldsymbol{x}) = -\delta(\boldsymbol{x}) \tag{A1}$$

and is given by

$$\mathcal{G}(\boldsymbol{x}) = \frac{1}{4\pi |\boldsymbol{x}|}. \tag{A2}$$

1. Charged prolate spheroid

Any point $\boldsymbol{x}$ on a prolate spheroid S_p with semimajor axis a and aspect ratio $\kappa(>1)$, oriented along the unit vector $\boldsymbol{p}$ and centered at origin is given by

$$\boldsymbol{x}\cdot\left[\frac{1}{a^2}\boldsymbol{pp}+\frac{1}{a^2\kappa^{-2}}(\mathbb{1}-\boldsymbol{pp})\right]\cdot\boldsymbol{x}=1,\quad \boldsymbol{x}\in S_p. \tag{A3}$$

The boundary value problem to be solved for the potential field outside S_p is

$$\nabla^2\phi(\boldsymbol{x}) = 0, \tag{A4a}$$
$$\phi(\boldsymbol{x}) = \phi_0,\quad \boldsymbol{x}\in S_p, \tag{A4b}$$
$$\phi(\boldsymbol{x})\to 0\quad \text{as}\quad |\boldsymbol{x}|\to\infty. \tag{A4c}$$

The solution can be represented in terms of a uniform charge distribution located along the symmetry axis of S_p as [46]

$$\phi(\boldsymbol{x})=\phi_0\left\{\frac{2\pi}{\operatorname{arctanh} e}\int_{-ae}^{ae}\mathcal{G}(\boldsymbol{x}-\xi\boldsymbol{p})d\xi\right\}, \tag{A5}$$

where $e=\sqrt{1-b^2/a^2}$ is the eccentricity. The total charge Q on the surface of S_p is given by

$$Q=-\varepsilon_0\oint_{S_p}\hat{\boldsymbol{n}}\cdot\nabla\phi\, dS=-\varepsilon_0\int_{V_p}\nabla^2\phi\, d\tau = \left[\frac{4\pi a\varepsilon_0 e}{\operatorname{arctanh} e}\right]\phi_0, \tag{A6}$$

where ε_0 is the permittivity of the free space and $\hat{\boldsymbol{n}}$ is the outward normal vector to S_p and V_p is the volume inside S_p. Therefore, the capacitance $C\equiv Q/\phi_0$ of the perfectly conducting prolate spheroid S_p is given by [23,25–27]

$$C=\frac{4\pi a\varepsilon_0 e}{\operatorname{arctanh} e}. \tag{A7}$$

Note that $\lim_{e\to 0} C = 4\pi a\varepsilon_0$, which is the capacitance of a sphere of radius a.

2. Charged oblate spheroid

The singularity solution of an oblate spheroid can be derived from that of a prolate spheroid using the eccentricity transformation [29]

$$e\to\frac{ie}{\sqrt{1-e^2}}. \tag{A8}$$

Therefore, the potential field due to an isolated oblate spheroid described by Eq. (A3) with $\kappa<1$ is given by

$$\phi(\boldsymbol{x})=\phi_0\left\{\frac{2\pi}{\arcsin e}\int_{-ae/\kappa}^{ae/\kappa}\mathcal{G}(\boldsymbol{x}-i\xi\boldsymbol{p})d\xi\right\}. \tag{A9}$$

Note that for cartesian coordinates aligned such that the unit vector $\boldsymbol{p}$ is along the z axis, $\mathcal{G}(\boldsymbol{x}-i\xi\boldsymbol{p})$ gives rise to a term $\frac{1}{\sqrt{x^2+y^2+(z-i\xi)^2}}$, which is singular on the disk of radius ξ in the x-y plane ($z=0$), which corresponds to the singularity distribution for an oblate spheroid [22].

Correspondingly, the capacitance of an isolated oblate spheroid is given by [23,25–27]

$$C=\frac{4\pi a\varepsilon_0 e}{\kappa\arcsin e}. \tag{A10}$$

3. Grounded prolate spheroid in presence of a uniform electric field

The potential field in this case can be divided into two parts as $\phi=\phi^d+\phi^\infty$. Here ϕ^d is the disturbance potential produced by the grounded prolate spheroid so as to maintain zero potential on its surface and $\phi^\infty=-\boldsymbol{E}^\infty\cdot\boldsymbol{x}$, with $\boldsymbol{E}^\infty$ being the ambient uniform electric field. The boundary value problem to be solved for $\phi^d(\boldsymbol{x})$ outside S_p in this case is

$$\nabla^2\phi^d(\boldsymbol{x}) = 0, \tag{A11a}$$
$$\phi^d(\boldsymbol{x}) = \boldsymbol{E}^\infty\cdot\boldsymbol{x},\quad \boldsymbol{x}\in S_p, \tag{A11b}$$
$$\phi^d(\boldsymbol{x})\to 0\quad \text{as}\quad |\boldsymbol{x}|\to\infty. \tag{A11c}$$

The solution can be represented as [46]

$$\phi^d(\boldsymbol{x})=\boldsymbol{E}^\infty\cdot\left\{\frac{6\pi X_p^C}{e^3}\boldsymbol{p}\int_{-ae}^{ae}\xi\,\mathcal{G}(\boldsymbol{x}-\xi\boldsymbol{p})d\xi - \frac{3\pi Y_p^C}{e^3}(\mathbb{1}-\boldsymbol{pp})\cdot\nabla\int_{-ae}^{ae}(a^2e^2-\xi^2)\times\mathcal{G}(\boldsymbol{x}-\xi\boldsymbol{p})d\xi\right\}, \tag{A12}$$

where

$$X_p^C\equiv\frac{e^3}{3}(\operatorname{arctanh} e-e)^{-1}, \tag{A13a}$$
$$Y_p^C\equiv\frac{2e^3}{3}\left(\frac{e}{1-e^2}-\operatorname{arctanh} e\right)^{-1}. \tag{A13b}$$

The first integral term in Eq. (A12) represents a linear charge distribution along the symmetry axis, whereas the second integral term represents the parabolic distribution of dipole moments pointing perpendicular to the symmetry axis. Note that the charge distribution in the first integral term has nonzero dipole moment but zero net charge. The induced dipole moment $\boldsymbol{d}$ is given by

$$\boldsymbol{d}=-\varepsilon_0\oint_{S_p}\boldsymbol{x}\,\hat{\boldsymbol{n}}\cdot\nabla\phi\, dS=-\varepsilon_0\int_{V_p}[\nabla\phi+\boldsymbol{x}\,\nabla^2\phi]d\tau. \tag{A14}$$

The volume integral of the gradient term does not contribute since $\phi=0$ on S_p and

$$\int_{V_p}\nabla\phi\, d\tau=\oint_{S_p}\phi\hat{\boldsymbol{n}}\, dS=0. \tag{A15}$$

Therefore, the dipole moment is given by

$$\boldsymbol{d} = -\varepsilon_0\int_{V_p}\boldsymbol{x}\,\nabla^2\phi^d d\tau = 4\pi a^3\varepsilon_0\left[X_p^C\boldsymbol{pp}+Y_p^C(\mathbb{1}-\boldsymbol{pp})\right]\cdot\boldsymbol{E}^\infty. \tag{A16}$$

Note that $\lim_{e\to 0}X_p^C=\lim_{e\to 0}Y_p^C=1$ resulting in $\lim_{e\to 0}\boldsymbol{d}=4\pi a^3\varepsilon_0\boldsymbol{E}^\infty$ and we get the dipole moment of a sphere of radius a. We can rewrite Eq. (A12) in terms of the dipole moment $\boldsymbol{d}$ as

$$\phi^d(\boldsymbol{x})=\frac{3}{2a^3e^3\varepsilon_0}\boldsymbol{d}\cdot\boldsymbol{p}\int_{-ae}^{ae}\xi\,\mathcal{G}(\boldsymbol{x}-\xi\boldsymbol{p})d\xi$$

$$-\frac{3}{4a^3e^3\varepsilon_0}\boldsymbol{d}\cdot(\mathbb{1}-\boldsymbol{pp})\cdot\nabla_{\boldsymbol{x}}\int_{-ae}^{ae}(a^2e^2-\xi^2)\times\mathcal{G}(\boldsymbol{x}-\xi\boldsymbol{p})d\xi. \tag{A17}$$

4. Grounded oblate spheroid in presence of a uniform electric field

We again use the eccentricity transformation (A8) to obtain the dipole moment $\boldsymbol{d}$ and disturbance potential field $\phi^d(\boldsymbol{x})$ due to a grounded oblate spheroid in the presence of a uniform background electric field $\boldsymbol{E}^\infty$. The dipole moment is given by

$$\boldsymbol{d}=4\pi a^3\varepsilon_0\left[X_o^C\boldsymbol{pp}+Y_o^C(\mathbb{1}-\boldsymbol{pp})\right]\cdot\boldsymbol{E}^\infty, \tag{A18}$$

where

$$X_o^C\equiv\frac{e^3}{3}[e(1-e^2)-(1-e^2)^{3/2}\arcsin e]^{-1}, \tag{A19a}$$

$$Y_o^C\equiv\frac{2e^3}{3}[e(1-e^2)^2-(1-e^2)^{3/2}\arcsin e]^{-1}. \tag{A19b}$$

The disturbance potential field is given by

$$\phi^d(\boldsymbol{x})=\frac{3\kappa^3}{2a^3e^3\varepsilon_0}\left\{\boldsymbol{d}\cdot\boldsymbol{p}\int_{-ae/\kappa}^{ae/\kappa}-i\xi\,\mathcal{G}(\boldsymbol{x}-i\xi\boldsymbol{p})d\xi-\frac{1}{2}\boldsymbol{d}\cdot(\mathbb{1}-\boldsymbol{pp})\cdot\nabla_{\boldsymbol{x}}\int_{-ae/\kappa}^{ae/\kappa}\left(\frac{a^2e^2}{\kappa^2}-\xi^2\right)\times\mathcal{G}(\boldsymbol{x}-i\xi\boldsymbol{p})d\xi\right\}. \tag{A20}$$

APPENDIX B: FAXÉN LAWS FOR ARBITRARY SHAPED CONDUCTORS IN ELECTROSTATICS

Faxén laws for electrostatics can be derived analogously to those in microhydrodynamics [22], using the reciprocal theorem. The electrostatic counterpart for spheres is detailed in [24], and we extend this framework to arbitrarily shaped conductors. Let ϕ_1 and ϕ_2 be two fields in the same domain D. The reciprocal theorem states that

$$\int_D\phi_2\nabla^2\phi_1d\tau-\int_D\phi_1\nabla^2\phi_2d\tau=\oint_{\partial D}\phi_2\nabla\phi_1\cdot\boldsymbol{n}\,dS-\oint_{\partial D}\phi_1\nabla\phi_2\cdot\boldsymbol{n}\,dS, \tag{B1}$$

where $\boldsymbol{n}$ is the normal vector to the boundary of the domain D, denoted by ∂D, pointing away from D. In the context of a conductor placed in a potential field, D is the region in $\mathbb{R}^3$ bounded by the surface of the conductor and a large sphere "at infinity.".

1. Faxén law for total charge and potential on a conductor

We follow the approach of [22] to relate the total charge Q on the surface of a conductor to its surface potential V in the presence of an arbitrary background potential field $\boldsymbol{\phi}^\infty(\boldsymbol{x})$, such that $\phi^\infty(\boldsymbol{x})\sim O(1/|\boldsymbol{x}|)$ as $\boldsymbol{x}$ goes to infinity. Let us denote the surface of an arbitrary shaped conductor by S_p. Note that total charge on S_p due to a potential $\phi(\boldsymbol{x})$ outside it, is given by

$$Q=-\varepsilon_0\oint_{S_p}\nabla\phi\cdot\hat{\boldsymbol{n}}\,dS, \tag{B2}$$

where $\hat{\boldsymbol{n}}$ is the outward pointing normal vector to S_p and ε_0 is the permittivity of free space.

We use the reciprocal theorem with the details of the two fields as follows:

(1) Take ϕ_1 to be the potential field satisfying the Laplace equation outside the isolated conductor with $\phi_1=\phi_{10}$ on S_p, where ϕ_{10} is some constant and ϕ_1 goes to zero at infinity. This is a case of an isolated conductor with some charge Q_1 on its surface given by $Q_1=C\phi_{10}$, where C is the capacitance of the conductor.

(2) Take ϕ_2 to be the potential field given by the solution of $\nabla^2\phi_2(\boldsymbol{x})=-Q'\varepsilon_0^{-1}\,\delta(\boldsymbol{x}-\boldsymbol{y})$, where $\boldsymbol{y}\in D$, with $\phi_2=V$ on S_p. Here the ambient potential field $\phi_2^\infty(\boldsymbol{x})$ is given by a point charge located at $\boldsymbol{y}$ and the conductor produces a disturbance field in order to satisfy the boundary condition on its surface. Let Q_2 be the charge on the conductor, which is to be determined using the reciprocal theorem.

Using Eqs. (B1) and (B2), we have [48]

$$Q'\phi_1(\boldsymbol{y})=Q_1V-Q_2\phi_{10}\Rightarrow Q_2\phi_{10}=C\phi_{10}V-Q'\phi_1(\boldsymbol{y}). \tag{B3}$$

Now, $\phi_1(\boldsymbol{y})$ can be represented in terms of a singularity solution as

$$\phi_1(\boldsymbol{y})=\phi_{10}\mathcal{F}_V\{\mathcal{G}(\boldsymbol{y}-\boldsymbol{\xi})\}=\phi_{10}\mathcal{F}_V\{\mathcal{G}(\boldsymbol{\xi}-\boldsymbol{y})\}. \tag{B4}$$

Here $\mathcal{F}_V$ is the corresponding linear functional and $\boldsymbol{\xi}$ represents the region inside the conductor over which the singularities are distributed. Using Eqs. (B3) and (B4), we have

$$Q_2=CV-Q'\mathcal{F}_V\{\mathcal{G}(\boldsymbol{\xi}-\boldsymbol{y})\}=CV-\mathcal{F}_V\left\{\phi_2^\infty(\boldsymbol{\xi})\right\}. \tag{B5}$$

Here we have used the fact that $Q'\mathcal{G}(\boldsymbol{\xi}-\boldsymbol{y})=\phi_2^\infty(\boldsymbol{\xi})$. However, all ambient fields $\phi^\infty(\boldsymbol{x})$ that decay at infinity and satisfy the Laplace equation can be constructed using an appropriate set of point charges. Therefore, Eq. (B5) applies to a general ambient field $\phi^\infty(\boldsymbol{x})$. Thus, the relation between charge Q on a conductor and the potential V on its surface in the presence of a background potential field $\phi^\infty(\boldsymbol{x})$ is given by

$$Q=CV-\mathcal{F}_V\{\phi^\infty(\boldsymbol{\xi})\}. \tag{B6}$$

This result can be directly applied to the bodies with known singularity solution of the form given in Eq. (B4). In particular, for a prolate spheroid with semimajor axis a, eccentricity e, and orientation vector $\boldsymbol{p}$ we have the singularity representation given by Eq. (A5) and capacitance by Eq. (A7). Therefore, the charge Q on the prolate spheroid in the presence of a background potential field ϕ^∞ is given by

$$Q=\frac{4\pi a\varepsilon_0e}{\operatorname{arctanh}e}\left\{V-\frac{1}{2ae}\int_{-ae}^{ae}\phi^\infty(\boldsymbol{x}_c+\xi\boldsymbol{p})d\xi\right\}, \tag{B7}$$

where $c=ae$ and $\boldsymbol{x}_c$ denotes the center of the prolate spheroid.

Similarly, the charge relation for an oblate spheroid with semimajor axis a and orientation vector $\boldsymbol{p}$ in the presence of a

background potential field ϕ^∞ is given by

$$Q = \frac{4\pi a\varepsilon_0 e}{\kappa \arcsin e}\left\{V - \frac{\kappa}{2ae}\int_{-ae/\kappa}^{ae/\kappa} \phi^\infty(\boldsymbol{x}_c + i\xi\boldsymbol{p})d\xi\right\}. \quad \text{(B8)}$$

2. Faxén law for induced dipole moment on a conductor

To relate the induced dipole moment $\boldsymbol{d}$ on a conductor due to the presence of an ambient potential field $\phi^\infty(\boldsymbol{x})$, we again use the reciprocal theorem with the details of the two fields as follows:

(1) Take ϕ_1 to be the potential field satisfying the Laplace equation outside the isolated conductor with $\phi_1 = \boldsymbol{E}_{10}^\infty \cdot \boldsymbol{x}$ on S_p, where $\boldsymbol{E}_{10}^\infty$ is a constant electric field and ϕ_1 goes to zero at infinity. This is a case of the disturbance potential produced by a grounded isolated conductor placed in a uniform ambient field $\boldsymbol{E}_{10}^\infty$.

(2) Take ϕ_2 to be the potential field given by the solution of $\nabla^2\phi_2(\boldsymbol{x}) = -Q'\varepsilon_0^{-1}\,\delta(\boldsymbol{x}-\boldsymbol{y})$, where $\boldsymbol{y} \in D$, with $\phi_2 = 0$ on S_p. The goal is to determine the induced dipole moment $\boldsymbol{d}_2$ in this case.

Applying the reciprocal theorem in these two fields gives

$$Q'\phi_1(\boldsymbol{y}) = \varepsilon_0 \boldsymbol{E}_{10}^\infty \cdot \oint_{S_p} \boldsymbol{x}\nabla\phi_2 \cdot \hat{\boldsymbol{n}}\, dS = -\boldsymbol{E}_{10}^\infty \cdot \boldsymbol{d}_2, \quad \text{(B9)}$$

where we have used the fact that the surface charge density on the conductor is given by $\sigma_2 = -\varepsilon_0\nabla\phi_2 \cdot \hat{\boldsymbol{n}}$ and dipole moment $\boldsymbol{d}_2$ is simply the first moment of this charge density on the conductor. Now, $\phi_1(\boldsymbol{y})$ can be represented in terms of singularity solution as

$$\phi_1(\boldsymbol{y}) = \boldsymbol{E}_{10}^\infty \cdot \mathcal{F}_E\{\mathcal{G}(\boldsymbol{y}-\boldsymbol{\xi})\} = \boldsymbol{E}_{10}^\infty \cdot \mathcal{F}_E\{\mathcal{G}(\boldsymbol{\xi}-\boldsymbol{y})\}. \quad \text{(B10)}$$

Here $\mathcal{F}_E$ is the corresponding linear functional and $\boldsymbol{\xi}$ represents the region inside the conductor over which the singularities are distributed. Using this in Eq. (B9) and factoring out $\boldsymbol{E}_{10}^\infty$, we have

$$\boldsymbol{d}_2 = -\mathcal{F}_E\{Q'\mathcal{G}(\boldsymbol{\xi}-\boldsymbol{y})\} = -\mathcal{F}_E\left\{\phi_2^\infty(\boldsymbol{\xi})\right\}, \quad \text{(B11)}$$

where ϕ_2^∞ is the ambient potential field in the second case. Again, for the general ambient field $\phi^\infty(\boldsymbol{x})$ constructed using an appropriate set of point charges, the dipole moment $\boldsymbol{d}$ on the conductor is simply given by

$$\boldsymbol{d} = -\mathcal{F}_E\{\phi^\infty(\boldsymbol{\xi})\}. \quad \text{(B12)}$$

This result can be directly applied to the bodies with a known singularity solution of the form given in Eq. (B10). In particular, for a prolate spheroid with semimajor axis a, eccentricity e, and orientation vector $\boldsymbol{p}$ we have the singularity representation given by Eq. (A12). Therefore, the induced dipole moment on the prolate spheroid in the presence of a background potential field ϕ^∞ is given by

$$\begin{aligned}\boldsymbol{d} = &-4\pi a^3\varepsilon_0\Bigg[\frac{3}{2a^3e^3}X_p^C\boldsymbol{p}\int_{-ae}^{ae}\xi\,\phi^\infty(\boldsymbol{x}_c+\xi\boldsymbol{p})d\xi\\ &+\frac{3}{4a^3e^3}Y_p^C(\mathbb{1}-\boldsymbol{pp})\cdot\nabla_{\boldsymbol{x}_c}\int_{-ae}^{ae}(a^2e^2-\xi^2)\\ &\times\,\phi^\infty(\boldsymbol{x}_c+\xi\boldsymbol{p})d\xi\Bigg]. \quad \text{(B13)}\end{aligned}$$

Similarly, the dipole moment of an oblate spheroid with semimajor axis a and orientation vector $\boldsymbol{p}$ in the presence of a background potential field ϕ^∞ is given by

$$\begin{aligned}\boldsymbol{d} = &-4\pi a^3\varepsilon_0\frac{3\kappa^3}{2a^3e^3}\Bigg[X_o^C\boldsymbol{p}\int_{-ae/\kappa}^{ae/\kappa}i\xi\phi^\infty(\boldsymbol{x}_c+i\xi\boldsymbol{p})d\xi\\ &+\frac{Y_o^C}{2}(\mathbb{1}-\boldsymbol{pp})\cdot\nabla_{\boldsymbol{x}_c}\int_{-ae/\kappa}^{ae/\kappa}\left(\frac{a^2e^2}{\kappa^2}-\xi^2\right)\\ &\times\,\phi^\infty(\boldsymbol{x}_c+i\xi\boldsymbol{p})d\xi\Bigg]. \quad \text{(B14)}\end{aligned}$$

APPENDIX C: ELECTROSTATIC INTERACTIONS USING THE METHOD OF REFLECTIONS

The exact way to incorporate electrostatic interaction between conductors would require obtaining a harmonic potential field which satisfies the constant potential boundary conditions on the surface of each conductor. This problem is barely tractable for two spheres, and hence we need to resort to some approximate methods such as the method of reflections for more complex shapes like spheroids.

Method of reflections is an iterative scheme widely used in microhydrodynamics to calculate hydrodynamic interactions between widely separated bodies [22]. This method produces a perturbation series in terms of the order a/R where a is the typical size of the objects and R is their typical separation. The method is described in [22] and is outlined for an electrostatic interaction between two conductors as follows.

In the zeroth-order approximation, the solution for two conductors (denoted S_1 and S_2) that are far apart is obtained by simply adding the potential fields of each isolated conductor, meaning the electrostatic interactions between them are ignored. Let ϕ_1 and ϕ_2 be two potential fields such that

$$\phi_1(\boldsymbol{x}) = V_1, \quad \boldsymbol{x} \in S_1, \quad \text{(C1a)}$$

$$\phi_2(\boldsymbol{x}) = V_2, \quad \boldsymbol{x} \in S_2. \quad \text{(C1b)}$$

However, $\phi = \phi_1 + \phi_2$ does not satisfy the boundary conditions on either of the surfaces. In fact, the error in the boundary condition on S_α is $\phi_{3-\alpha}(\boldsymbol{x})$, which is of the order of a/R. The fields $\phi_1(\boldsymbol{x})$ and $\phi_2(\boldsymbol{x})$ are called the first *incident fields* on the conductors S_2 and S_1, respectively. Now, S_1 produces a disturbance field ϕ_{21} and S_2 produces a disturbance field ϕ_{12} such that

$$\phi_{21}(\boldsymbol{x}) = -\phi_2(\boldsymbol{x}), \quad \boldsymbol{x} \in S_1, \quad \text{(C2a)}$$

$$\phi_{12}(\boldsymbol{x}) = -\phi_1(\boldsymbol{x}), \quad \boldsymbol{x} \in S_2. \quad \text{(C2b)}$$

These disturbance fields are called the *reflected fields,* which accounts for the correction in the boundary conditions. Now, $\phi = \phi_1 + \phi_2 + \phi_{21} + \phi_{12}$ is a better approximation to the complete solution because the error in the boundary conditions is now $O(\phi_{12}) \sim O(\phi_{21})$, which takes contributions from higher multipole moments and decays faster than a/R. This procedure can be iterated with the reflected fields from one conductor being incident on the other conductor and producing subsequent reflected fields. We shall apply this method up to second reflections in the case of interacting spheroids.

1. Far-field interaction of two prolate spheroids

Consider two prolate spheroids S_1 and S_2 with semimajor axes a_1 and a_2, eccentricities e_1 and e_2, position vectors $\boldsymbol{x}_1$ and $\boldsymbol{x}_2$, and orientations $\boldsymbol{p}_1$ and $\boldsymbol{p}_2$, respectively. Faxén laws [see Eq. (B7)] can be used to relate the potentials V_1 and V_2 on the surfaces of the spheroids to their total charges Q_1 and Q_2, respectively. The ambient field around the first spheroid is generated by the second spheroid and can be expressed perturbatively using the method of reflections. The same approach applies to the second spheroid, where its ambient field is influenced by the first spheroid. Using Eq. (B7), we have for the first spheroid

$$V_1 = Q_1 \frac{\operatorname{arctanh} e_1}{4\pi a_1 \varepsilon_0 e_1} + \frac{1}{2a_1 e_1}\int_{-a_1e_1}^{a_1e_1} \phi_2^{\infty}(\boldsymbol{x}_1 + \xi_1 \boldsymbol{p}_1) d\xi_1, \tag{C3a}$$

$$V_2 = Q_2 \frac{\operatorname{arctanh} e_2}{4\pi a_2 \varepsilon_0 e_2} + \frac{1}{2a_2 e_2}\int_{-a_2e_2}^{a_2e_2} \phi_1^{\infty}(\boldsymbol{x}_2 + \xi_1 \boldsymbol{p}_2) d\xi_1. \tag{C3b}$$

Using the method of reflections, we have

$$\phi_1^{\infty}(\boldsymbol{y}) = \phi_1(\boldsymbol{y}) + \phi_{21}(\boldsymbol{y}) + \phi_{121}(\boldsymbol{y})..., \tag{C4a}$$

$$\phi_2^{\infty}(\boldsymbol{y}) = \phi_2(\boldsymbol{y}) + \phi_{12}(\boldsymbol{y}) + \phi_{212}(\boldsymbol{y})... . \tag{C4b}$$

Here $\phi_1(\boldsymbol{y})$ and $\phi_2(\boldsymbol{y})$ are the zeroth-order disturbance fields, $\phi_{21}(\boldsymbol{y})$ and $\phi_{12}(\boldsymbol{y})$ are the first reflection fields, and $\phi_{121}(\boldsymbol{y})$ and $\phi_{212}(\boldsymbol{y})$ are the second reflection fields produced by S_1 and S_2, respectively.

The zeroth-order solution to the problem is

$$V_1^{(0)} = Q_1 \frac{\operatorname{arctanh} e_1}{4\pi a_1 \varepsilon_0 e_1}, \quad V_2^{(0)} = Q_2 \frac{\operatorname{arctanh} e_2}{4\pi a_2 \varepsilon_0 e_2}. \tag{C5}$$

Since ϕ_1 and ϕ_2 are the potentials due to isolated spheroids S_1 and S_2, they are given by Eqs. (A5) and (A6) as

$$\phi_1(\boldsymbol{y}) = \frac{Q_1}{2\varepsilon_0 a_1 e_1}\int_{-a_1e_1}^{a_1e_1} \mathcal{G}(\boldsymbol{y} - \boldsymbol{x}_1 - \xi_1 \boldsymbol{p}_1) d\xi_1, \tag{C6a}$$

$$\phi_2(\boldsymbol{y}) = \frac{Q_2}{2\varepsilon_0 a_2 e_2}\int_{-a_2e_2}^{a_2e_2} \mathcal{G}(\boldsymbol{y} - \boldsymbol{x}_2 - \xi_1 \boldsymbol{p}_2) d\xi_1. \tag{C6b}$$

The first-order correction comes through the first reflection as

$$V_1^{(1)} = \frac{1}{2a_1 e_1}\int_{-a_1e_1}^{a_1e_1} \phi_2(\boldsymbol{x}_1 + \xi_1 \boldsymbol{p}_1) d\xi_1, \tag{C7a}$$

$$V_2^{(1)} = \frac{1}{2a_2 e_2}\int_{-a_2e_2}^{a_2e_2} \phi_1(\boldsymbol{x}_2 + \xi_1 \boldsymbol{p}_2) d\xi_1, \tag{C7b}$$

with the first reflection fields ϕ_{21} and ϕ_{12} represented to the leading order in a/R by the dipole moments $\boldsymbol{d}_1^{(1)}$ and $\boldsymbol{d}_2^{(1)}$. The explicit expression for the first reflection field ϕ_{12} by spheroid S_2 is [see Eq. (A17)]

$$\phi_{12}(\boldsymbol{y}) = \frac{3}{2a_2^3 e_2^3 \varepsilon_0}\Bigg[\boldsymbol{d}_2^{(1)} \cdot \boldsymbol{p}_2 \int_{-a_2e_2}^{a_2e_2} \xi_2\, \mathcal{G}(\boldsymbol{y} - \boldsymbol{x}_2 - \xi_2 \boldsymbol{p}_2) d\xi_2 - \frac{\boldsymbol{d}_2^{(1)}}{2} \cdot (\mathbb{1} - \boldsymbol{p}_2\boldsymbol{p}_2) \cdot \nabla_y \int_{-a_2e_2}^{a_2e_2} \left(a_2^2 e_2^2 - \xi_2^2\right) \times \mathcal{G}(\boldsymbol{y} - \boldsymbol{x}_2 - \xi_2 \boldsymbol{p}_2) d\xi_2 \Bigg]. \tag{C8}$$

The dipole moment $\boldsymbol{d}_2^{(1)}$ is given by the Faxén laws as [see Eq. (B13)]

$$\boldsymbol{d}_2^{(1)} = -4\pi a_2^3 \frac{3}{2a_2^3 e_2^3}\Bigg[X_2^C \boldsymbol{p}_2 \int_{-c_2}^{c_2} \xi_2\, d\xi_2 \int_{a_1e_1}^{a_1e_1} \frac{Q_1}{2a_1 e_1} \times \mathcal{G}(\boldsymbol{x}_2 + \boldsymbol{\xi}_2 - \boldsymbol{x}_1 - \boldsymbol{\xi}_1)\, d\xi_1 + \frac{Y_2^C}{2}(\mathbb{1} - \boldsymbol{p}_2\boldsymbol{p}_2) \cdot \nabla_{\boldsymbol{x}_2} \times \int_{-a_2e_2}^{a_2e_2} \left(a_2^2 e_2^2 - \xi_2^2\right) \int_{a_1e_1}^{a_1e_1} \frac{Q_1}{2a_1 e_1} \times \mathcal{G}(\boldsymbol{x}_2 + \boldsymbol{\xi}_2 - \boldsymbol{x}_1 - \boldsymbol{\xi}_1) d\xi_1 \Bigg], \tag{C9}$$

where we have used Eq. (C6) for $\phi_1(\boldsymbol{y})$ in place of ϕ^{∞} in Eq. (B13). The corresponding first reflection field $\phi_{21}(\boldsymbol{y})$ and the dipole moment $\boldsymbol{d}_1^{(1)}$ is obtained by simply switching the labels 1 and 2.

The next order correction comes through the second reflection as

$$V_1^{(2)} = \frac{1}{2a_1 e_1}\int_{-a_1e_1}^{a_1e_1} \phi_{12}(\boldsymbol{x}_1 + \xi_1 \boldsymbol{p}_1) d\xi_1, \tag{C10a}$$

$$V_2^{(2)} = \frac{1}{2a_2 e_2}\int_{-a_2e_2}^{a_2e_2} \phi_{21}(\boldsymbol{x}_2 + \xi_1 \boldsymbol{p}_2) d\xi_1, \tag{C10b}$$

with the second reflection fields ϕ_{121} and ϕ_{212} represented to the leading order in a/R by the dipole moments $\boldsymbol{d}_1^{(2)}$ and $\boldsymbol{d}_2^{(2)}$. These dipole moments can again be obtained using Faxén laws [Eq. (B13)] with first reflection fields in place on ϕ^{∞}.

Therefore, up to second reflections, the potentials on the surface of the spheroids are related to their respective total charges as $V_\alpha = V_\alpha^{(0)} + V_\alpha^{(1)} + V_\alpha^{(2)}$, $\alpha \in \{1, 2\}$. These interaction potentials are accurate up to $O(a^4/R^4)$.

2. Far-field interaction of a prolate spheroid and a sphere

Knowing the procedure for two spheroids, it is easy to look at a special case where the second spheroid is a sphere. This simplification is analytically tractable to obtain closed-form expressions without losing the flavor of anisotropy in the problem. Consider a spheroid S_1 centered at $\boldsymbol{x}_1$ with semimajor axis a, aspect ratio κ, eccentricity $e \equiv \sqrt{1 - \kappa^{-2}}$, and orientation vector $\boldsymbol{p}$, carrying total charge Q_1. The second conductor is a sphere S_2 centered at $\boldsymbol{x}_2$ with radius γa and total charge Q_2. The relative separation vector between them is $\boldsymbol{x}_{21} \equiv \boldsymbol{x}_2 - \boldsymbol{x}_1 \equiv -\boldsymbol{x}_{12}$. The relation between the surface potentials of S_1 and S_2 can be found by either taking limit $e_2 \to 0$ in the previous analysis or by applying the method of reflection to this system. The results up to the second reflection are stated as follows:

$$V_1 = \frac{Q_1}{4\pi a \varepsilon_0}\left(\frac{\operatorname{arctanh} e}{e}\right) + V_1^{(1)} + V_1^{(2)}, \tag{C11a}$$

$$V_2 = \frac{Q_2}{4\pi \varepsilon_0 \gamma a} + V_2^{(1)} + V_2^{(2)}, \tag{C11b}$$

where

$$V_1^{(1)} = \frac{Q_2}{2ae\varepsilon_0}\int_{-ae}^{ae} \mathcal{G}(\boldsymbol{x}_{12}+\xi\boldsymbol{p})d\xi, \tag{C12a}$$

$$V_2^{(1)} = \frac{Q_1}{2ae\varepsilon_0}\int_{-ae}^{ae} \mathcal{G}(\boldsymbol{x}_{21}-\xi\boldsymbol{p})d\xi, \tag{C12b}$$

and

$$V_1^{(2)} = -\frac{1}{2ae\varepsilon_0}\int_{-ae}^{ae} \boldsymbol{d}_2^{(1)}\cdot\nabla_{\boldsymbol{x}_1}\mathcal{G}(\boldsymbol{x}_{12}+\xi\boldsymbol{p})d\xi, \tag{C13a}$$

$$V_2^{(2)} = \frac{3}{2a^3e^3\varepsilon_0}\int_{-ae}^{ae} \boldsymbol{d}_1^{(1)}\cdot\Big\{\boldsymbol{p}\,\xi\,\mathcal{G}(\boldsymbol{x}_{21}-\xi\boldsymbol{p}) - \frac{1}{2}(a^2e^2-\xi^2)(\mathbb{1}-\boldsymbol{pp})\cdot\nabla_{\boldsymbol{x}_2}\mathcal{G}(\boldsymbol{x}_{21}-\xi\boldsymbol{p})\Big\}d\xi. \tag{C13b}$$

Here the dipole moments are given by

$$\boldsymbol{d}_1^{(1)} = -4\pi a^3 Q_2 \frac{3}{2a^3e^3}\int_{-ae}^{ae}\Big\{X_p^C\boldsymbol{p}\,\xi\,\mathcal{G}(\boldsymbol{x}_{12}+\xi\boldsymbol{p}) + \frac{1}{2}Y_p^C(a^2e^2-\xi^2)(\mathbb{1}-\boldsymbol{pp})\cdot\nabla_{\boldsymbol{x}_1}\mathcal{G}(\boldsymbol{x}_{12}+\xi\boldsymbol{p})\Big\}d\xi, \tag{C14a}$$

$$\boldsymbol{d}_2^{(1)} = -4\pi\gamma^3 a^3 Q_1 \frac{1}{2ae}\nabla_{\boldsymbol{x}_2}\int_{-ae}^{ae}\mathcal{G}(\boldsymbol{x}_2-\boldsymbol{x}_1-\xi\boldsymbol{p})d\xi. \tag{C14b}$$

These line integrals over $\mathcal{G}$ can be computed analytically [46,49]. After some algebra, we arrive at the closed-form expressions for the potentials given by

$$V_1^{(1)} = \frac{Q_2}{4\pi a\varepsilon_0}\frac{1}{2e}\ln\left(\frac{z_{12}-ae-R_-}{z_{12}+ae-R_+}\right), \tag{C15a}$$

$$V_2^{(1)} = \frac{Q_1}{Q_2}V_1^{(1)}, \tag{C15b}$$

where

$$R_\pm \equiv \sqrt{\rho_{12}^2+(z_{12}\pm ae)^2},$$
$$\rho_{12}^2 \equiv \boldsymbol{x}_{12}\cdot(\mathbb{1}-\boldsymbol{pp})\cdot\boldsymbol{x}_{12}, \quad z_{12}\equiv\boldsymbol{x}_{12}\cdot\boldsymbol{p}. \tag{C16}$$

The second-order corrections are given by

$$V_1^{(2)} = -\frac{Q_1}{4\pi a\varepsilon_0}\frac{a^2\gamma^3}{4e^2}\left[\left(\frac{1}{R_-}-\frac{1}{R_+}\right)^2+\rho_{12}^2 \times\left(\frac{1}{R_+(z_{12}+ae-R_+)}-\frac{1}{R_-(z_{12}-ae-R_-)}\right)^2\right], \tag{C17}$$

$$V_2^{(2)} = -\frac{Q_2}{4\pi a\varepsilon_0}\frac{9}{4a^2e^6}\left[X_p^C\left\{R_--R_+ + z_{12}\ln\left(\frac{z_{12}-ae-R_-}{z_{12}+ae-R_+}\right)\right\}^2 + \frac{Y_p^C}{4}\left\{\frac{z_{12}}{\rho_{12}}(R_--R_+)+\frac{ae}{\rho_{12}}(R_-+R_+) - \rho_{12}\ln\left(\frac{z_{12}-ae-R_-}{z_{12}+ae-R_+}\right)\right\}^2\right]. \tag{C18}$$

Recall that X_p^C and Y_p^C are given by Eq. (A13).

3. Far-field interaction of a oblate spheroid and a sphere

The eccentricity transformation (A8) allows us to directly obtain the surface potential from the prolate spheroid and sphere case, given below.

$$V_1 = \frac{Q_1}{4\pi a\varepsilon_0}\left(\frac{\kappa\arcsin e}{e}\right)+V_1^{(1)}+V_1^{(2)}, \tag{C19a}$$

$$V_2 = \frac{Q_2}{4\pi\varepsilon_0\gamma a}+V_2^{(1)}+V_2^{(2)}. \tag{C19b}$$

The first-order corrections are

$$V_1^{(1)} = \frac{Q_2}{4\pi a\varepsilon_0}\frac{\kappa}{e}\operatorname{arccot}\left(\frac{z_{12}-u}{v-ae/\kappa}\right), \tag{C20a}$$

$$V_2^{(1)} = \frac{Q_1}{Q_2}V_1^{(1)}, \tag{C20b}$$

where

$$u \equiv \sqrt{\frac{\mu}{2}+\sqrt{\frac{\mu^2}{4}+\frac{a^2e^2}{\kappa^2}z_{12}^2}},$$
$$\mu \equiv |\boldsymbol{x}_{12}|^2-\frac{a^2e^2}{\kappa^2}, \quad v\equiv\frac{aez_{12}}{\kappa u}. \tag{C21}$$

The second-order corrections are given by

$$V_1^{(2)} = -\frac{Q_1}{4\pi a\varepsilon_0}\frac{\kappa^2a^2\gamma^3}{4e^2}\left[\left(\frac{2v}{u^2+v^2}\right)^2 + \rho_{12}^2\left\{\frac{4ae\kappa^{-1}z_{12}-2(z_{12}v+ae\kappa^{-1}u)}{(u^2+v^2)[(z_{12}-u)^2+(ae\kappa^{-1}-v)^2]}\right\}^2\right], \tag{C22a}$$

$$V_2^{(2)} = -\frac{Q_2}{4\pi a\varepsilon_0}\frac{9\kappa^6}{a^2e^6}\left[X_o^C\left\{v-z_{12}\operatorname{arccot}\left(\frac{z_{12}-u}{v-ae\kappa^{-1}}\right)\right\}^2 + \frac{1}{4}Y_o^C\left\{\frac{ae\kappa^{-1}u-z_{12}v}{\rho_{12}}-\rho_{12}\operatorname{arccot}\left(\frac{z_{12}-u}{v-ae\kappa^{-1}}\right)\right\}^2\right]. \tag{C22b}$$

Recall that X_o^C and Y_o^C are given by Eq. (A19).

APPENDIX D: BOUNDARY INTEGRAL FORMULATION FOR ARBITRARY SHAPED CONDUCTORS IN ELECTROSTATICS

The external Dirichlet problem of N charged conductors in an unbounded medium in electrostatics is

$$\nabla^2\phi(\boldsymbol{x}) = 0, \tag{D1a}$$

$$\phi(\boldsymbol{x}_s) = V_\alpha, \quad \text{for } \boldsymbol{x}_s\in S_\alpha, \tag{D1b}$$

$$\phi(\boldsymbol{x})\to 0 \quad \text{as} \quad |\boldsymbol{x}|\to\infty, \tag{D1c}$$

where S_α denotes the surface of conductor α and $\alpha \in \{1, 2, ..., N\}$. In a manner similar to microhydrodynamics [22,31–33,50], the potential field $\phi(\boldsymbol{x}_0)$ can be represented in terms of a double-layer potential as

$$\varepsilon_0\phi(\boldsymbol{x}_0) = -2\sum_{\alpha=1}^{N}\oint_{S_\alpha} q_\alpha(\boldsymbol{x})\hat{\boldsymbol{n}}_\alpha \cdot \nabla_{\boldsymbol{x}}\mathcal{G}(\boldsymbol{x}, \boldsymbol{x}_0)dS_\alpha(\boldsymbol{x}) + \sum_{\alpha=1}^{N} Q_\alpha \mathcal{G}(\boldsymbol{x}_0, \boldsymbol{x}_\alpha). \tag{D2}$$

Here the first term denotes the double-layer potential, q_α is an unknown double-layer density, $\hat{\boldsymbol{n}}_\alpha$ is outward normal to the surface S_α, Q_α is the total charge on S_α, and $\boldsymbol{x}_\alpha$ is a point lying inside the conductor S_α. The unknown double-layer densities q_α are determined using the boundary conditions

$$\lim_{\boldsymbol{x}_0 \to S_\alpha^+} \phi(x_0) = V_\alpha, \quad \alpha \in \{1, 2, \ldots N\}, \tag{D3}$$

where $\boldsymbol{x}_0 \to S_\alpha^+$ denotes the approach to the surface S_α is from the outside of the surface, i.e., along $\hat{\boldsymbol{n}}_\alpha$ [51]. The second term involving Q_α is needed to complete the double-layer representation [22,50]. Applying the boundary condition in Eq. (D2), we obtain a second kind of integral equations given by

$$\sum_{\beta=1}^{N}\left(\mathcal{L}^d_{\alpha\beta} + \delta_{\alpha\beta}\right) q_\beta(\boldsymbol{x}_s) = \sum_{\beta=1}^{N} Q_\beta \mathcal{G}(\boldsymbol{x}_s, \boldsymbol{x}_\alpha) - \varepsilon_0 V_\alpha, \tag{D4}$$

where $\alpha \in \{1, 2, .., .N\}$ and $\mathcal{L}^d_{\alpha\beta}$ is the double-layer operator given by

$$\mathcal{L}^d_{\alpha\beta} q_\beta(\boldsymbol{x}_s) \equiv 2\oint_{S_\beta} q_\beta(\boldsymbol{x})\,\hat{\boldsymbol{n}}_\beta \cdot \nabla_{\boldsymbol{x}}\mathcal{G}(\boldsymbol{x}, \boldsymbol{x}_s)dS_\beta(\boldsymbol{x}), \tag{D5}$$

$\boldsymbol{x}_s \in S_\alpha$. Given total charges Q_α on each conductor, we are required to obtain the potentials V_α on the surface of each conductor. Using $\mathcal{L}^d_{\alpha\beta} c = -c\,\delta_{\alpha\beta}$ where c is a constant function defined on the surface of S_β, we see that (D4) has no unique solution. Since V_α's are unknown, one chooses the solutions q_α such that the projection of q_α onto the subspace of constant functions (which are eigenfunctions of $\mathcal{L}^d_{\alpha\beta}$) is exactly V_α. The corresponding projection operator is given by

$$\mathcal{P}^c_{\alpha\beta} q_\beta \equiv \frac{1}{|S_\alpha|}\delta_{\alpha\beta}\oint_{S_\beta} q_\beta(\boldsymbol{x})dS_\beta(\boldsymbol{x}), \tag{D6}$$

where $|S_\alpha|$ is the surface area of conductor S_α. Therefore, choosing $\sum_{\beta=1}^{N}\mathcal{P}^c_{\alpha\beta}q_\beta = V_\alpha$ not only fixes the nonuniqueness problem but also determines the V_α's once the solutions q_α are known. This leads to a well-defined second kind integral equation given by

$$\sum_{\beta=1}^{N}\left(\mathcal{L}^d_{\alpha\beta} + \mathcal{P}^c_{\alpha\beta} + \delta_{\alpha\beta}\right) q_\beta(\boldsymbol{x}_s) = \sum_{\beta=1}^{N} Q_\beta \mathcal{G}(\boldsymbol{x}_s, \boldsymbol{x}_\alpha), \tag{D7}$$

$\alpha \in \{1, 2, ..., N\}$, with the potential fields given by

$$\varepsilon_0 V_\alpha = \frac{1}{|S_\alpha|}\oint_{S_\alpha} q_\alpha(\boldsymbol{x})dS_\alpha(\boldsymbol{x}), \quad \alpha \in \{1, 2, ..., N\}. \tag{D8}$$

Using arguments similar to those in [22,50], it can be shown that the spectrum of $\mathcal{L}^d_{\alpha\beta} + \mathcal{P}^c_{\alpha\beta}$ lies in the interval $(-1, 1)$ and hence Eq. (D7) admits a unique solution which can be obtained through Picard iterations.

To solve the boundary integral equations (D7) for a spheroid and a sphere we perform the surface integrals using Gaussian quadrature defined on the surfaces [31,37] using the parametric equations of the surfaces. GMRES [31,36] is used to converge to the solutions.

[1] T. B. Jones, *Electromechanics of Particles* (Cambridge University Press, Cambridge, 1995).

[2] C.-S. Wang, Electrostatic forces in fibrous filters—a review, Powder Technol. **118**, 166 (2001).

[3] S. Sun, P. Poudel, E. Alexov, and L. Li, Electrostatics in computational biophysics and its implications for disease effects, Int. J. Mol. Sci. **23**, 10347 (2022).

[4] T. D. Edwards and M. A. Bevan, Controlling colloidal particles with electric fields, Langmuir **30**, 10793 (2014).

[5] H. R. Pruppacher and J. D. Klett, *Microphysics of Clouds and Precipitation* (Springer Science & Business Media, Berlin, 2012).

[6] P. Patra and A. Roy, Brownian coagulation of like-charged aerosol particles, Phys. Rev. Fluids **7**, 064308 (2022).

[7] P. Patra, D. L. Koch, and A. Roy, Collision efficiency of like-charged spheres settling in a quiescent environment, J. Fluid Mech. **968**, A22 (2023).

[8] J. Lekner, Regions of attraction between like-charged conducting spheres, Am. J. Phys. **84**, 474 (2016).

[9] N. Thiruvenkadam, P. Patra, V. K. Puttanna, and A. Roy, Pair trajectories of uncharged conducting spheres in an electric field, Phys. Fluids **35**, 033311 (2023).

[10] M. H. Davis, Two charged spherical conductors in a uniform electric field: Forces and field strength, Q. J. Mech. Appl. Math. **17**, 499 (1964).

[11] J. Dhanasekaran, A. Roy, and D. L. Koch, Collision rate of bidisperse, hydrodynamically interacting spheres settling in a turbulent flow, J. Fluid Mech. **912**, A5 (2021).

[12] P. K. Wang and W. Ji, Collision efficiencies of ice crystals at low–intermediate reynolds numbers colliding with supercooled cloud droplets: A numerical study, J. Atmos. Sci. **57**, 1001 (2000).

[13] A. Naso, J. Jucha, E. Lévêque, and A. Pumir, Collision rate of ice crystals with water droplets in turbulent flows, J. Fluid Mech. **845**, 615 (2018).

[14] S. Twomey, The electrification of individual cloud droplets, Tellus A **8**, 445 (1956).

[15] N. Krasnogorskaya, Warm cloud electricity, Planetary Electrodyn. **1**, 427 (1969).

[16] S. A. Colgate and J. M. Romero, Charge versus drop size in an electrified cloud, J. Geophys. Res. **75**, 5873 (1970).

[17] T. Takahashi, Riming electrification as a charge generation mechanism in thunderstorms, J. Atmos. Sci. **35**, 1536 (1978).

[18] C. Saunders and S. Peck, Laboratory studies of the influence of the rime accretion rate on charge transfer during crystal/graupel collisions, J. Geophys. Res.: Atmos. **103**, 13949 (1998).
[19] M. Y. Luque, F. Nollas, R. G. Pereyra, R. E. Bürgesser, and E. E. Ávila, Charge separation in collisions between ice crystals and a spherical simulated graupel of centimeter size, J. Geophys. Res.: Atmos. **125**, e2019JD030941 (2020).
[20] J. Lekner, Electrostatics of two charged conducting spheres, Proc. R. Soc. A **468**, 2829 (2012).
[21] I. N. Derbenev, A. V. Filippov, A. J. Stace, and E. Besley, Electrostatic interactions between spheroidal dielectric particles, J. Chem. Phys. **152**, 024121 (2020).
[22] S. Kim and S. J. Karrila, *Microhydrodynamics: Principles and Selected Applications* (Butterworth-Heinemann, Oxford, UK, 2013).
[23] L. D. Landau, J. S. Bell, M. Kearsley, L. Pitaevskii, E. Lifshitz, and J. Sykes, *Electrodynamics of Continuous Media* (Elsevier, New York, 2013), Vol. 8.
[24] R. Bonnecaze and J. Brady, A method for determining the effective conductivity of dispersions of particles, Proc. R. Soc. A **430**, 285 (1990).
[25] A. Zangwill, *Modern Electrodynamics* (Cambridge University Press, Cambridge, 2013).
[26] J. A. Stratton, *Electromagnetic Theory* (Wiley, New York, 2007), Vol. 33.
[27] J. Lekner, *Electrostatics of Conducting Cylinders and Spheres* (AIP, Melville, NY, 2021).
[28] The more familiar capacitance matrix is simply the inverse of the potential matrix.
[29] L. F. Shatz, Singularity method for oblate and prolate spheroids in stokes and linearized oscillatory flow, Phys. Fluids **16**, 664 (2004).
[30] A. S. Khair, Electrostatic forces on two almost touching nonspherical charged conductors, J. Appl. Phys. **114**, 134906 (2013).
[31] J. Bagge, Accurate quadrature and fast summation in boundary integral methods for Stokes flow, Ph.D. thesis, KTH Royal Institute of Technology, 2023.
[32] A. Prosperetti, *Computational Methods for Multiphase Flow* (Cambridge University Press, Cambridge, 2009).
[33] C. Pozrikidis, *A Practical Guide to Boundary Element Methods with the Software Library BEMLIB* (CRC, Boca Raton, FL, 2002).
[34] P.-G. Martinsson, *Fast Direct Solvers for Elliptic PDEs* (SIAM, Philadelphia, 2019).
[35] M. Gorman, X. Ruan, and R. Ni, Electrostatic interactions between rough dielectric particles, Phys. Rev. E **109**, 034902 (2024).
[36] Y. Saad and M. H. Schultz, GMRES: A generalized minimal residual algorithm for solving nonsymmetric linear systems, SIAM J. Sci. Stat. Comput. **7**, 856 (1986).
[37] G. H. Golub and J. H. Welsch, Calculation of Gauss quadrature rules, Math. Comput. **23**, 221 (1969).
[38] Although the accuracy of the expression requires the radius of the sphere to be much less than the separation between the particles.
[39] C. I. Trombley and M. L. Ekiel-Jeżewska, Stable configurations of charged sedimenting particles, Phys. Rev. Lett. **121**, 254502 (2018).
[40] J. M. Crowley, Viscosity-induced instability of a one-dimensional lattice of falling spheres, J. Fluid Mech. **45**, 151 (1971).
[41] R. Chajwa, N. Menon, S. Ramaswamy, and R. Govindarajan, Waves, algebraic growth, and clumping in sedimenting disk arrays, Phys. Rev. X **10**, 041016 (2020).
[42] D. L. Koch and E. S. Shaqfeh, The instability of a dispersion of sedimenting spheroids, J. Fluid Mech. **209**, 521 (1989).
[43] J. Bec, H. Homann, and S. S. Ray, Gravity-driven enhancement of heavy particle clustering in turbulent flow, Phys. Rev. Lett. **112**, 184501 (2014).
[44] J. Meibohm, V. Pandey, A. Bhatnagar, K. Gustavsson, D. Mitra, P. Perlekar, and B. Mehlig, Paths to caustic formation in turbulent aerosols, Phys. Rev. Fluids **6**, L062302 (2021).
[45] The supporting data can be found at https://github.com/harshit314/ElectrostaticsData/releases/tag/v1.1.
[46] A. Alawneh and R. Kanwal, Singularity methods in mathematical physics, SIAM Rev. **19**, 437 (1977).
[47] A. Roy, S. Kramel, U. Menon, G. A. Voth, and D. L. Koch, Orientation of finite reynolds number anisotropic particles settling in turbulence, J. Non-Newtonian Fluid Mech. **318**, 105048 (2023).
[48] We have used the fact that the fields involved in the problems decay fast enough far from the conductor so as to have zero contribution from the surface "at infinity."
[49] A. T. Chwang and T. Y.-T. Wu, Hydromechanics of low-reynolds-number flow. part 2. singularity method for stokes flows, J. Fluid Mech. **67**, 787 (1975).
[50] C. Pozrikidis, *Boundary Integral and Singularity Methods for Linearized Viscous Flow* (Cambridge University Press, Cambridge, 1992).
[51] The direction of approach matters because the double-layer potential has a jump discontinuity across the surface.